Eindhoven University of Technology

MASTER

Interaction between plasma and neutrals near the divertor : the effect of particle and energy reflection

Minea, T.

Award date:
2013

Link to publication

Disclaimer
This document contains a student thesis (bachelor's or master's), as authored by a student at Eindhoven University of Technology. Student theses are made available in the TU/e repository upon obtaining the required degree. The grade received is not published on the document as presented in the repository. The required complexity or quality of research of student theses may vary by program, and the required minimum study period may vary in duration.

General rights
Copyright and moral rights for the publications made accessible in the public portal are retained by the authors and/or other copyright owners and it is a condition of accessing publications that users recognise and abide by the legal requirements associated with these rights.

- Users may download and print one copy of any publication from the public portal for the purpose of private study or research.
- You may not further distribute the material or use it for any profit-making activity or commercial gain

Eindhoven University of Technology

Master Thesis

Interaction between plasma and neutrals near the divertor: the effect of particle and energy reflection

Author:
T. Minea

Supervisors:
Dr. G.J. van Rooij
Dr. R. Jaspers
Prof. dr. W.J. Goedheer
Drs. N. den Harder

A thesis submitted in fulfillment of the requirements for the degree of Master of Science

in the

Science and Technology of Nuclear Fusion
Applied Physics

August 2013

EINDHOVEN UNIVERSITY OF TECHNOLOGY

Abstract

Eindhoven University of Technology
Applied Physics

Master of Science

Interaction between plasma and neutrals near the divertor: the effect of particle and energy reflection

by T. Minea

In plasma physics, material walls are traditionally regarded as perfect sinks for charged particles and their energy. This work considers the special case that arises when the wall efficiently reflects the neutralized plasma particles (due to a large mass difference between incident particles and lattice atoms) and the upstream plasma is of sufficiently high density to stop these reflected neutrals. The kinetic energy of the reflected particles will thus be a considerable portion of the energy that their parent ions had gained in the acceleration over the plasma sheath that naturally interfaces the plasma and the wall. It may therefore be even larger than the local thermal energy and locally heat the ions in collisions. This effect was for the first time experimentally observed in the linear plasma generator Pilot-PSI at DIFFER and is relevant for the situation that is expected in next generation fusion devices. A single fluid 1D numerical model is developed to study the effect of energy reflection from the target and subsequent thermalization in the upstream plasma. Firstly, the effect on the upstream plasma flow is characterized and compared with new flow velocity measurements in Pilot-PSI. It demonstrates that the commonly encountered flow velocities of around half the sound speed in the upstream plasma can fully be explained by the interaction with the neutral source at the target. Subsequently, the effect on the power density transferred to the wall as well as the kinetic energy of the incident heavy particles is evaluated as a function of the energy reflection fraction, plasma conditions and plasma sheath voltage to evaluate the importance for plasma surface interaction in fusion devices.

Contents

Chapter 1

Introduction

A plasma is a hot gas consisting of charged and neutral particles which exhibits collective behavior due to the significant presence of free charge. It is known that most of the matter in the universe exists in a state of plasma. Plasmas may exist in a wide range of densities and temperatures: from astrophysical region to man made plasmas as shown in Figure 1.1.

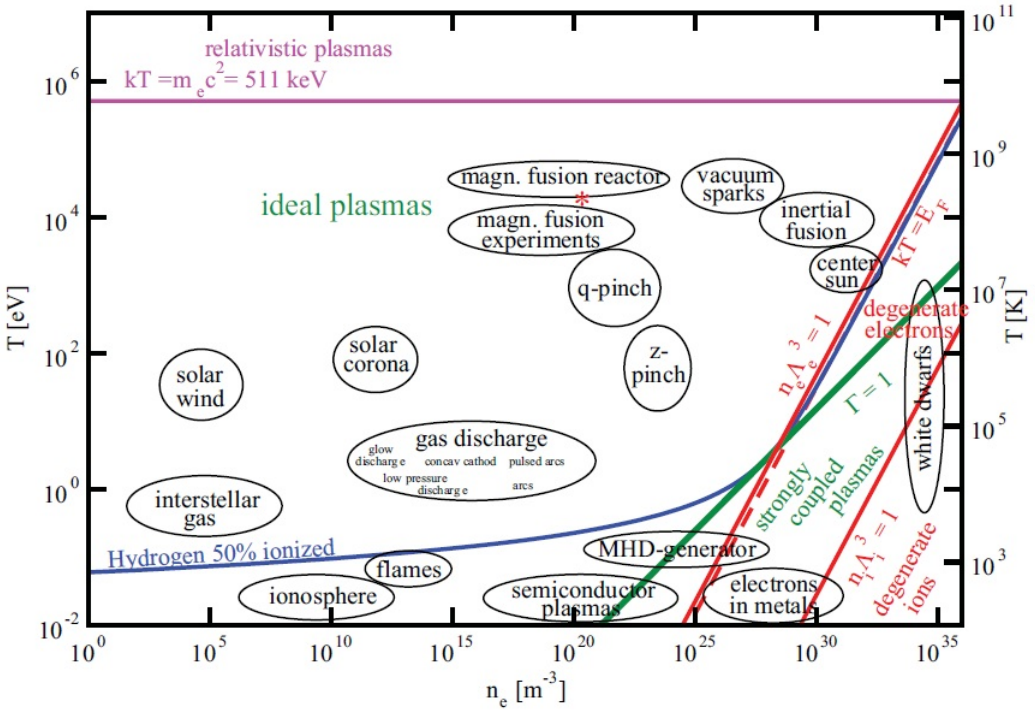

FIGURE 1.1: Temperatures and densities of various astrophysical and laboratory plasmas [1]

An interesting application of man-made plasma with huge benefits is the achievement of a so called *burning plasma* based on fusion reactions with the main purpose of net energy production which has remained an unachieved goal for physicists for more than 50 years [2]. Having the possibility of endless supplies of energy and also environmental friendly, that is, no carbon emissions and far less waste material than produced by present nuclear fission power plants remains the ultimate dream for plasma physicists. Although, the situation is about to change due to ongoing construction of ITER (a 500-MW heat generating fusion plant using toroidal magnetic confinement geometry: *a tokamak*) which is envisaged to represent the breakthrough from experimental studies of plasma physics to full-scale electricity producing power plants.

The fusion reaction is a nuclear process in which two light nuclei collide together to form a heavier nucleus while releasing energy during the process. In order for this to happen, very high densities and temperatures are needed within a sufficient confinement time. The easiest approach in terms of highest reaction rate is provided by the reaction between the two hydrogen isotopes deuterium and tritium, which produces helium (α particle) and a neutron. The neutrons capture 80% of the released energy and the α particles get the remaining of 20%.

The key concept of the tokamak is represented by its magnetic field topology , as shown in Figure 1.2. The combination of a toroidal magnetic field (induced by external field coils) with a poloidal field (from an electric current through the plasma), produces helical field lines. Both magnetic field lines and current density lines lie on so-called *nested flux surfaces*. Parallel to the field lines, transport of heat and particles is very fast which results in constant temperature and pressure at the surface. On the other hand, in the radial direction, i.e., perpendicular to the field lines, transport is slow, being possible through e.g. collisions. In reality, the radial transport is enhanced by change in the field topology due to various instabilities and by turbulence. As a result more particles and energy than expected in a purely collisional picture end up hitting the wall thus reducing confinement. The latter reason gives a hint why fusion is being more difficult than initially foreseen.

A successful approach for limiting the deleterious effect from plasma wall interaction as well as fuel cycle is given by the *divertor* configuration Figure 1.3. By using a set of coils a null point, or an X point, is created in the magnetic topology allowing the particles and heat to be exhausted over the region called divertor. Furthermore, the magnetic boundary between confined plasma and edge/divertor plasma is called *separatrix* or Last Close Flux Surface (LCFS). In addition, between the LCFS and the vessel wall the so called Scrape-off Layer (SOL) is formed.
Through the SOL, heat and particles are being removed out from the reactor main

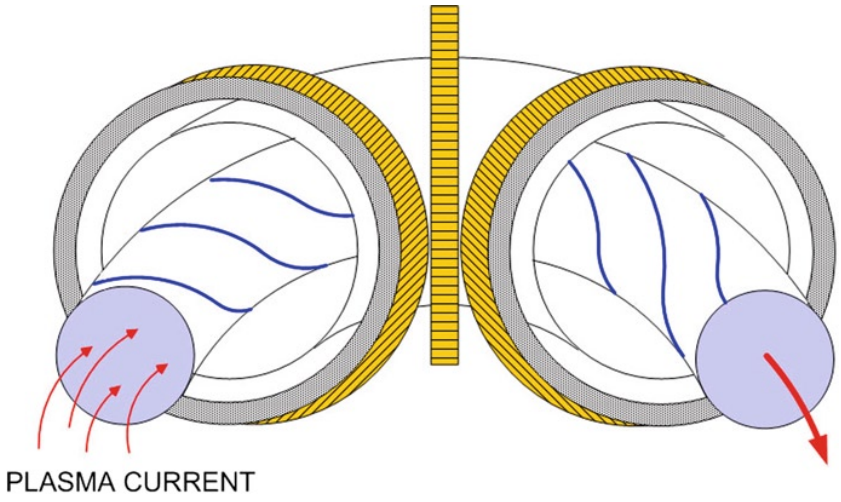

FIGURE 1.2: This figure shows an ideal magnetic field topology in a tokamak: helical field lines are created by external coils and plasma current.[2]

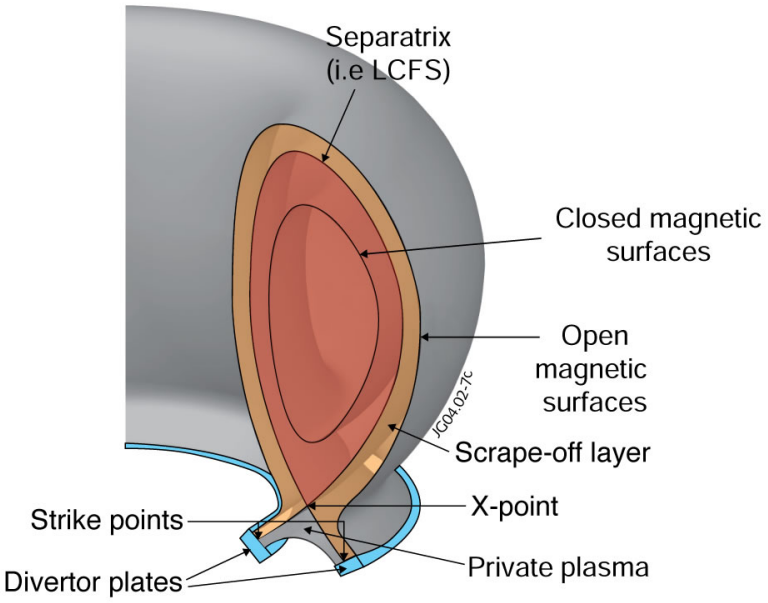

FIGURE 1.3: This picture shows a poloidal cross section of a tokamak in divertor configuration together with the most important parts where the plasma surface interaction takes place : at the divertor plates. The divertor can be seen as an extension of the scrape off layer where all the core heat is conducted and exhausted in the end. Its structure also prevents neutrals from leaving it and going back into the core plasma. [3]

plasma and directed towards the divertor plates. There will have to withstand steady state fluxes in the order of 10 $\mathrm{MWm^{-2}}$ and 10^{24} $\mathrm{m^{-2}s^{-1}}$, respectively in e.g. ITER. These values are not trivial and finding a lasting solution for the divertor remains a challenge in the fusion community. At present, the two linear plasma generators Pilot-PSI and Magnum-PSI at the FOM-institute DIFFER are able to mimic the divertor as expected in ITER and aid in finding such solutions.

1.1 Motivation

Due to cost reduction as well as high tritium retention issues for the carbon based divertor parts, a transition towards a full tungsten divertor has happened in ITER without a trial stage of a mixed tungsten-carbon divertor as initially foreseen. In Figure 1.4 we see a substantial increase in both particle and energy reflection coefficients as well as a peak shifting towards lower impinging ions energies for carbon versus tungsten plates.In other words, whilst predominantly molecules would return with a kinetic energy determined by the surface temperature from a carbon divertor surface, mainly energetic atoms will return from a tungsten surface. Connecting this effect with the high plasma density, i.e. $n_e > 10^{20}$, near the divertor results in a strong coupling of the high energetic backscattered neutrals and the plasma ions via a resonant process called charge exchange. It is the aim of the present work to isolate this effect and assess its effect on the case of plasma parameters and consequent plasma surface interaction in linear devices such as Pilot / Magnum - PSI and from there to extrapolate to plasma surface interaction in ITER.

In a picture without neutrals, the pre-sheath region of the plasma in front of the target would be infinite and the plasma would have a flow speed equal v= c_s, where c_s is the sound speed. This is only the case of a strong convective plasma flow like the one in Pilot-PSI and Magnum-PSI. That is of course valid within the imposed boundary conditions at the target, i.e. according to the Bohm criterion plasma needs to reach sound speed at the sheath entrance Now what happens if a neutral source is taken into account at the target?

The neutrals can take the form of a "cushion" in front of the target and this is the low energetic population, or the backscattered neutrals from the target, which is a high energy ($\propto$ sheath's energy) population. The neutrals can resonantly interact with the ions in the plasma via charge exchange (CX) processes by **adding energy** back into it and removing momentum. A schematic view is drawn in Figure 1.5.

A new finding in this context, hinted at by experimental results from Pilot-PSI [5], is the mechanism of capturing of energy carried by the reflected neutrals by the upstream plasma, which increases the upstream heavy particle temperature and therewith elevates the flow velocity of the heavy particles at the sheath entrance. This effect is due to the fact that the ions are accelerated over the plasma sheath before being neutralized at the target, and therefore the reflected neutrals will have a larger kinetic energy that the thermal energy of the upstream ions. Furthermore, clear evidence of different plasma ion temperature behavior for different target materials has been found in [6], which enforces the hypothesis of reflected neutrals leading to plasma heating. An immediate

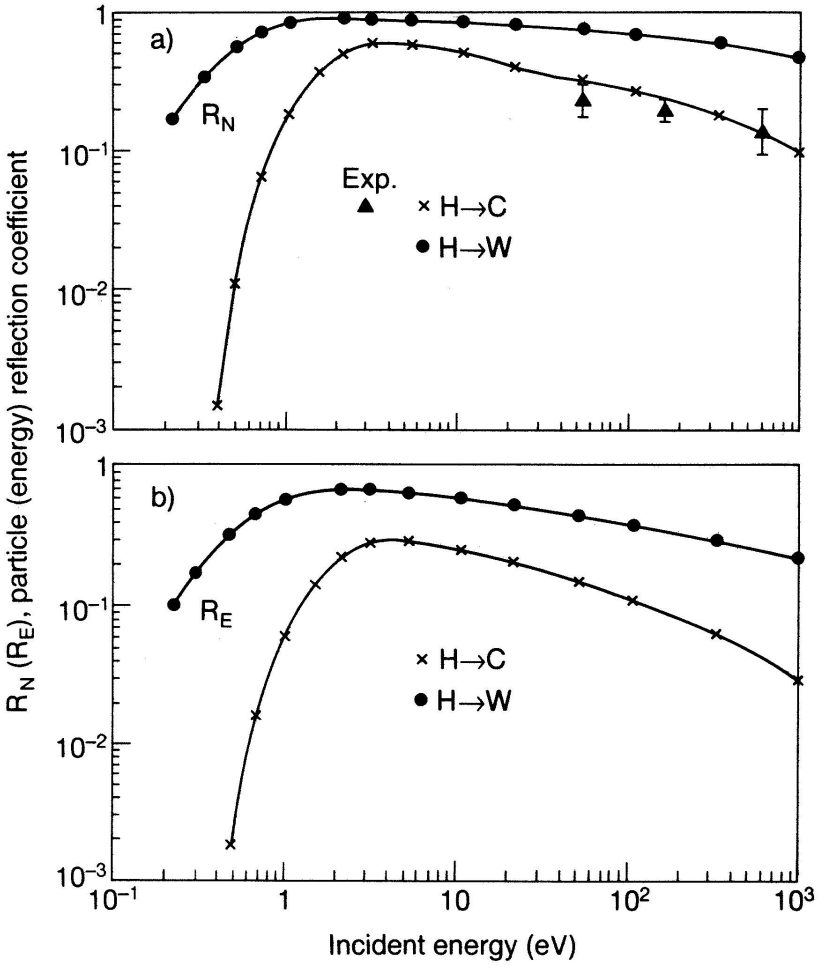

FIGURE 1.4: This figure shows particle (a) and energy reflection coefficients (b) for hydrogen ions incident on carbon and tungsten solid surfaces as a function of the impact energy.[4]

consequence of this effect is the impossibility of an accurate computation of the reaction rates close to the surface of the divertor for example.

Within the framework of this thesis an interpretative 1D modeling study has been performed on the plasma flow characteristics to Pilot-PSI like devices. Already at this point, one may ask what is the necessity of a simple model when there are already advanced codes available [7] such as the in house developed B 2.5 Eunomia . The answer is rather intuitive, that is, to study the effect of various assumptions the large complex codes are not flexible enough. A simple 1D model can much better reveal the interplay between various parameters such as the relations proposed in the research questions. People often make "toy models" to get a better understanding. In B2.5-Eunomia, changing an assumption may come back as a change in radial profile, blurring the pure influence of the assumption on the electric field, for instance.

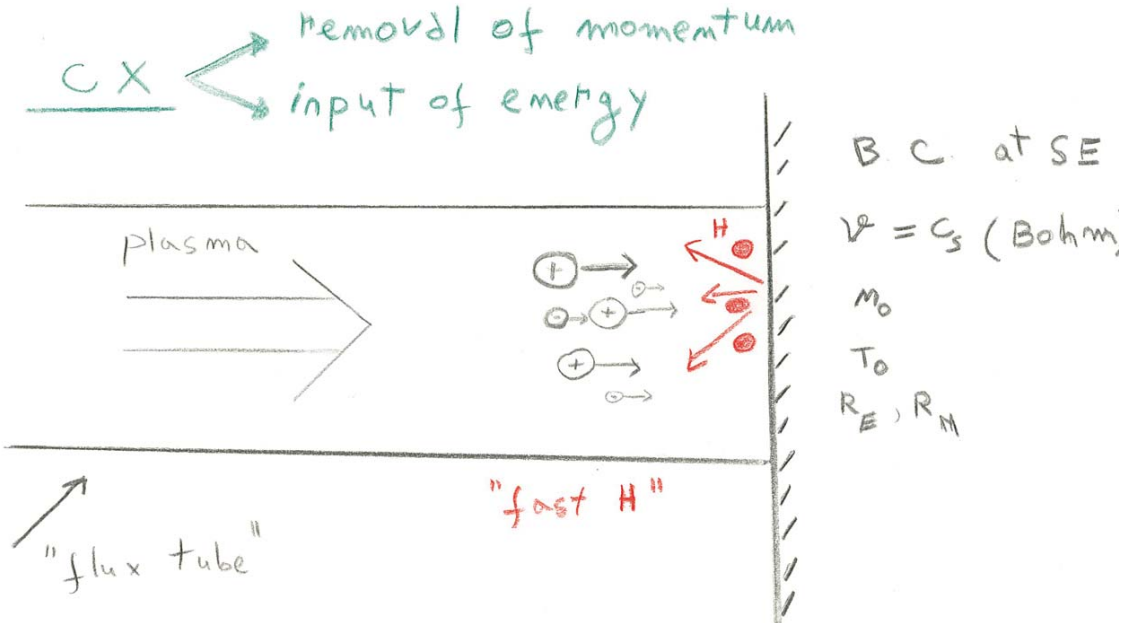

FIGURE 1.5: Hand drawing of plasma wall interaction. In this picture, hydrogen ions are being accelerated in a two stage process: firstly, the high energetic neutrals that come back into the plasma undergo a CX reaction from which a high energetic ion appears; secondly, this newly formed ion is the subject of a further plasma acceleration due to imperfect shielding of target potential

1.2 This thesis

The main research question of this project is :

How does the neutral source feed back to the upstream plasma and how does this alter Plasma Surface Interaction in ITER / Pilot / Magnum-PSI ?

In first instance, research is done specific for Pilot-PSI and Magnum-PSI, with focus on the effect on temperature, flow speed and target heat loads.
The emphasis lies on conditions that combine high energy reflection coefficients, i.e. metals with high Z number, with a strong coupling between neutrals and plasma particles, i.e. high plasma density $n_e > 10^{20}$. Although the work focuses on the experimental conditions of the in house linear plasma generators, it is on basis of the match in plasma parameter space, i.e. high density and low temperature, directly applicable to the ITER divertor. The ITER relevance lies in the fact that the strong coupling between neutrals and the plasma affects the heat losses to the strike point and the average energy per incoming particle. As such, it relates to key challenges of ITER such as heat loads on the divertor, sputtering and/or further plasma contamination.

This research project has two main parts. Firstly, an experimental approach to determine plasma flow velocities in Pilot-PSI. An experimental database on local particle flux measurements perform with an electrostatic probe embedded in the target of Pilot-PSI with corresponding upstream plasma conditions from Thomson scattering is achieved. In addition, the experiments serve to pinpoint the parameters space to benchmark the simulations. Probe measurements are combined with Thomson scattering results to determine plasma flow velocities. Independent, pressure measurements are performed to yield the same information.

Secondly, a theoretical modeling part is done where spatially resolved plasma profiles are obtained. The interpretative fluid modeling is devised in two stages. At first the plasma fluid equations are numerically solved in a frame where $T_e = T_i$. Subsequently, a hybrid 2 fluid model that allows for the electron and ion temperature unequilibrium is used to obtain insight into the possibility of local ion heating by energy exchange between the plasma and energetic reflected neutrals.

The numerical code for solving the explicit ODE system describing the plasma fluid equations is based on a first order backward finite difference approximation for the derivative, followed by a Newton iteration scheme. The code is implemented in the the Sundials toolbox [8] for Matlab which is based on the CVODE solvers for ordinary differential equations. It is noted that, CVODE is the same solver used in obtaining solutions of the plasma fluid equations within the UEDGE plasma simulator [9].

Chapter 2

Some background on the properties of the electrostatic plasma sheath and pre-sheath

2.1 Introduction

The first step in any evaluation of plasma in front of a surface and the resulting plasma surface interaction is the characterization of the electrostatic plasma sheath and pre-sheath that naturally form.
This chapter is mostly based on the description found in Chapter 2 of Stangeby's book *The plasma boundary of magnetic fusion devices*[10] and Chapter 11 of Bittencourt's *Fundamentals of Plasma Physics*[11].

2.2 Plasma Sheath

The physical mechanism behind the plasma sheath formation is easily understood starting from an initial picture in a bulk plasma at rest in which charge neutrality exists. Introducing a wall in this environment creates a sink for the plasma on which all charged particles are lost. The ions recombine at the wall and return into the plasma as neutrals whereas the electrons may either directly recombine or enter the conduction band provided the wall is a metal. The electrons and ions are initially described by Maxwellian distributions from which one gets the one way Maxwellian flux towards the immersed wall: $\Gamma_\alpha = \frac{1}{4} n_\alpha < v >_\alpha$, where n_α is the density and $< v >_\alpha$ is the average particle speed of the α species. Due to their large mass difference the electron and ion Maxwellian

fluxes to the wall will thus largely differ as well. Assuming temperature equilibrium between ions and electrons one finds that electron fluxes are ≈ 42 higher than ion fluxes (for hydrogen ions). As a result, the wall charges up negatively until an electric field is established that balances the two fluxes, namely the *ambipolar* electric field. At this point there is no net current drawn towards the wall, that is, the wall is *floating*.

The thickness of the layer of net space charge that sets up the ambipolar field is of the order of the Debye length $\lambda_D = \sqrt{\frac{\epsilon_0 T_e}{e^2 n_e}}$. The negative potential of the floating wall V_f is defined with respect to the sheath edge potential V_{se}. The plasma sheath is a positive charged region. From stability reasons, the ions must enter the sheath at sound velocity $c_s = \sqrt{\frac{T_e + \gamma \mathrm{T}_i}{m_i}}$, also called the Bohm criterion, and the existence of a pre-sheath is a must in the fulfilment of this criterion, i.e. to accelerate the ions from $v = 0$ in the upstream plasma to c_S near the target.[12].

Furthermore, the length of the pre-sheath is determined by the ion mean free path, by the ionization length or by the geometry of the system (i.e. the cases of spherical walls/probes). In addition, a magnetic pre-sheath will exists for configurations with oblique magnetic field to the wall.
In the case of Pilot-PSI plasma the pre-sheath is neutral dominated. A pre-sheath that is dominated by the neutral-ion interaction shows a variation in length according to the different values of the charge exchange mean free path. Measuring flow velocities at a fixed location from the target for various plasma conditions yields information of the pre-sheath behavior and ultimately on the neutral plasma interaction. To what extent this pre-sheath matches in length the ion-mean free path remains to be determined later in this report.

In this project there is no model of the sheath, since that would imply a different approach, i.e. a kinetic model, on a different length scale and that is beyond the scope of the present work. Still, boundary conditions, e.g. Bohm criterion, are used in the fluid simulations which implicitly require a zone of plasma acceleration, i.e. the so-called pre-sheath, to fulfil this criterion.

Chapter 3

Experimental Approach

3.1 Pilot-PSI

Pilot-PSI is a linear plasma generator that has an unique feature when it comes to plasma surface interaction: it can reach particle fluxes exceeding 10^{24} m^{-2} s^{-1} and temperatures in the interval of 0.1-5 eV which makes the device ITER relevant. During plasma operation, the vessel pressure is basically around 1 Pa. A cascaded arc source is used to produce the plasma by applying a high current between the cathodes and the anode of the source. The resulted plasma expands out into the vacuum vessel due to the pressure difference until it is confined by an axial magnetic filed. The magnetic field takes values from 0.2 T in continuous operation up to 1.6 T in short pulses. A diagram of Pilot-PSI is shown in Figure 3.1.

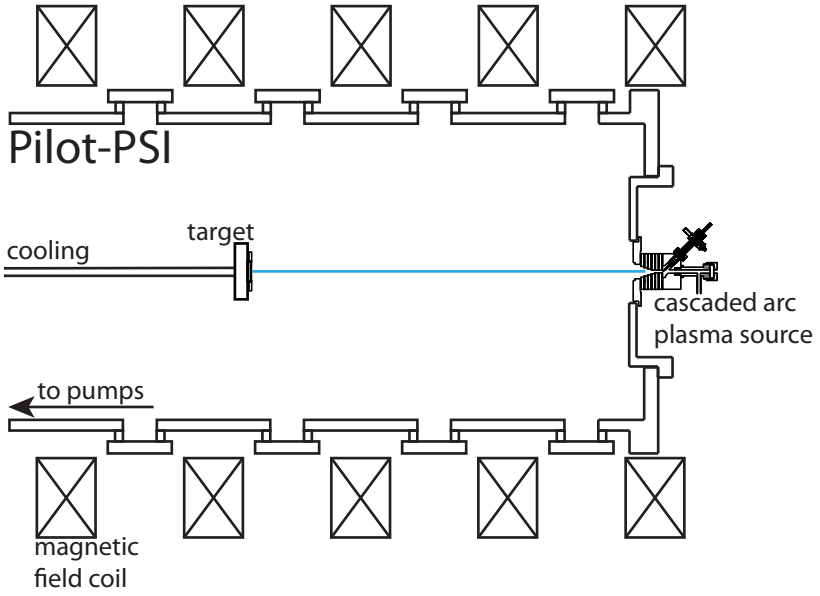

FIGURE 3.1: This figure shows a schematic representation of Pilot-PSI, a linear plasma generator designed for plasma surface interaction studies under extreme particle and heat loads (ITER relevant). Up to five surrounding coils create a homogeneous magnetic field that guide and confine the plasma created by the cascaded arc source to a specific target. In addition, booster pumps are used to maintain a constant low vessel pressure.

3.2 Thomson scattering

Insight into the main plasma parameters, namely, electron temperature and density in front of the target at ≈ 2 cm is obtained via a high resolution Thomson scattering (TS) system at Pilot-PSI. A detailed description about operating principles of a TS diagnostic as well as underlining theory can be found elsewhere [13]. Upon shining a laser through the plasma, light is scattered by the free electrons. The density of the electrons is proportional to the intensity of the scattered light while the temperature is proportional to the square root of the Doppler width of the acquired spectrum. The system can measure n_e and T_e with a spatial resolution of 0.6 mm and has an observational error of 3 % and 6 % for $n_e = 4 * 10^{-19}\ m^{-3}$. These errors decrease further with increasing density of the plasma.

3.3 Langmuir probe

The ratio between plasma flow velocity v and sound speed c_s defines the Mach number equation for the plasma column.

$$M = \frac{v}{c_s} \tag{3.1}$$

In order to obtain the Mach numbers, an insight into particle fluxes at the target should be established. Furthermore, the particle fluxes represent initial conditions for the $1-$D

model approach, which enhances their importance into the system.
Starting from the conservative form of the momentum equation, while assuming cold ions and isothermal conditions together with Bohm criterion, a half drop in density at the sheath edge is found. This approach results in a way of computing the particle flux at the sheath edge Γ_{se} .

$$p_e + p_i + mnv^2 = \text{constant} \tag{3.2}$$

$$n_0 T_e = n_{\text{se}} T_e + m n_{\text{se}} v_{\text{se}}^2 \tag{3.3}$$

$$\frac{n_0}{n_{\text{se}}} = 1 + \left(\frac{v_{\text{se}}}{c_s}\right)^2 \tag{3.4}$$

$$\Gamma_{\text{se}} = n_{\text{se}} v_{\text{se}} = \frac{1}{2} n_0 c_s \tag{3.5}$$

However, this approach is different from the experimental situation where ions are not cold and the bulk plasma is not at still. Another way of determining the ion fluxes at the target is with the help of a Langmuir probe.

The Langmuir probe consists of a conducting pin that is embedded in the target in the plasma, as shown in Figure 3.3, while sweeping the applied potential applied to the probe over a wide range and measuring the acquired current.The probe was negatively biased with a triple triangle voltage wave that reached -150 V for hydrogen and -100 for argon in order to avoid damaging the probe due to arcing near the target as shown in Figure 3.2.

By analyzing the resulted I-V characteristic various plasma parameters can be derived such as electron temperature and density or ion fluxes. Data analysis of Langmuir probes is cumbersome and not often straight forward especially when oblique magnetic field is present. However, for determining the ion fluxes the results are obtained quite easily. With respect to the mechanism of plasma sheath formation described in the previous section, the existence of an energy filter for the electrons was underlined. Therefore, by increasing further in magnitude the wall/probe potential even the high energetic electrons are repelled and what remains is a collection of ions only, the ion saturation current which is directly linked to ion particle flux Γ_i. Conservation of particle flux in between Thomson measuring position and target is assumed.

$$\Gamma_i = \frac{I_{\text{sat}}}{e A_{\text{probe}}} \tag{3.6}$$

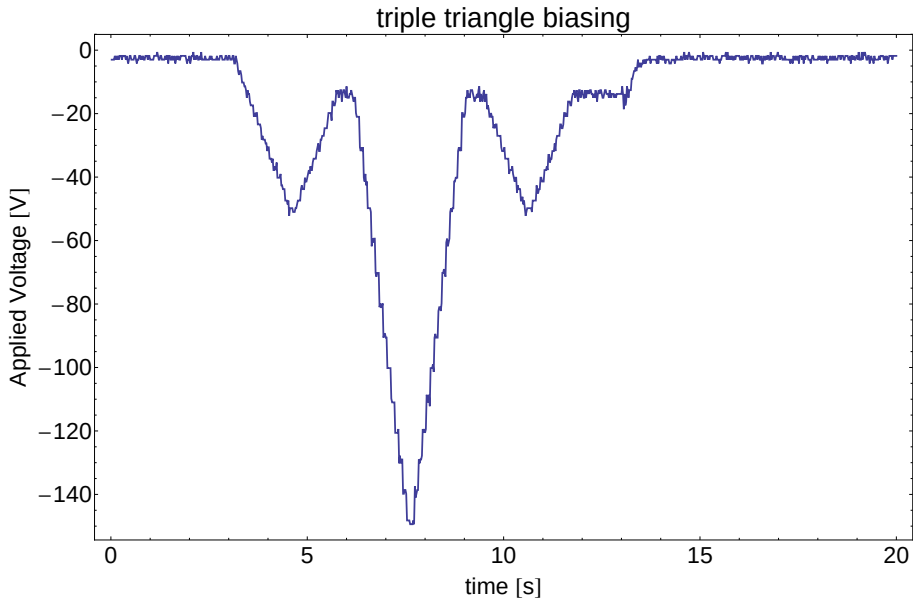

FIGURE 3.2: A biasing function profile used for the Langmuir probe experiment. The triple triangle function keeps the probe free of damage due to arcing and samples more points in the expected saturation limit range.

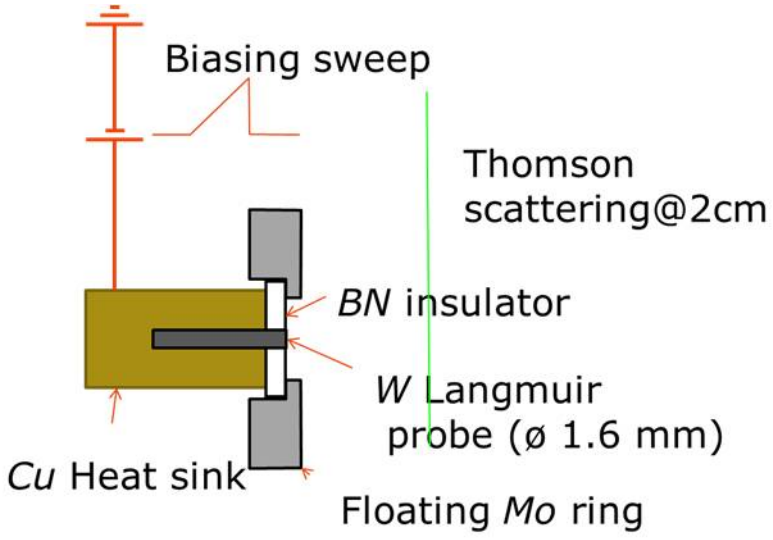

FIGURE 3.3: Schematic representation of Langmuir probe experiment. The probe consists of one conductor which is connected to a power supply and generates a voltage relative to the ground. Applying a negative voltage results in an ionic current.

3.4 Experimental campaigns

Experiments done on 20^{th} of September 2012 aimed at determining electron temperature and density for a large number of source parameters and magnetic field in order to create a database of plasma parameters which is subsequently used for measuring $I-V$ characteristics of the Langmuir probe. This was done due to the incompatibility of shining the laser through the plasma near the target (3^{rd} window) simultaneously with the immersion of the probe. Therefore, reproducibility of plasma parameters for same settings should be taken as an assumption.

Experiments done on 21^{st} of September 2012 consisted in recording the $I-V$ characteristics, with an oscilloscope, for the plasma parameters previously determined.

Chapter 4

Measurements of plasma flow velocities in Pilot-PSI

Typical TS profiles that were measured are shown in Figure 4.1. It is seen that the detection chord was not well centered with the plasma beam so that one edge of the beam profile was missing in these measurements. The peak density and temperature are still well determined, which were of main interest within the present context. We are interested in a flux tube that finds itself in the middle of the plasma beam. Therefore, it should have highest density and temperature. Taking the maximum value after performing a "moving median" on the data gives the final values that are used further in the analysis.

By varying the experimental parameters such as confining magnetic field, gas flow in the cascaded arc source and source current, electron temperatures of 0.4-2 eV and densities in the order of $0.8 - 3.8 \times 10^{20}$ m^3 were achieved, as is shown in Figure 4.2.

Typical $I - V$ characteristics are shown in Figure 4.3 and Figure 4.4 for both hydrogen and argon discharges. Both of these characteristics show a linear decreasing of current in the region where saturation is expected, that is, well bellow the floating potential. An explanation consists in a resistive behavior of the probe, since what we see is voltage driven. For example, a thin metallic layer of impurities might have adhered to the insulating surface around the wire. The saturation current is in such cases obtained from a linear fitting and an extrapolation towards the abscissa at 0 V as is indicated in the figures.

Basically, saturation currents are particle fluxes multiplied with electron charge and surface of the collection probe. Figure 4.5 shows a comparison between flux densities,calculated from the density and temperature measured with Thomson scattering as

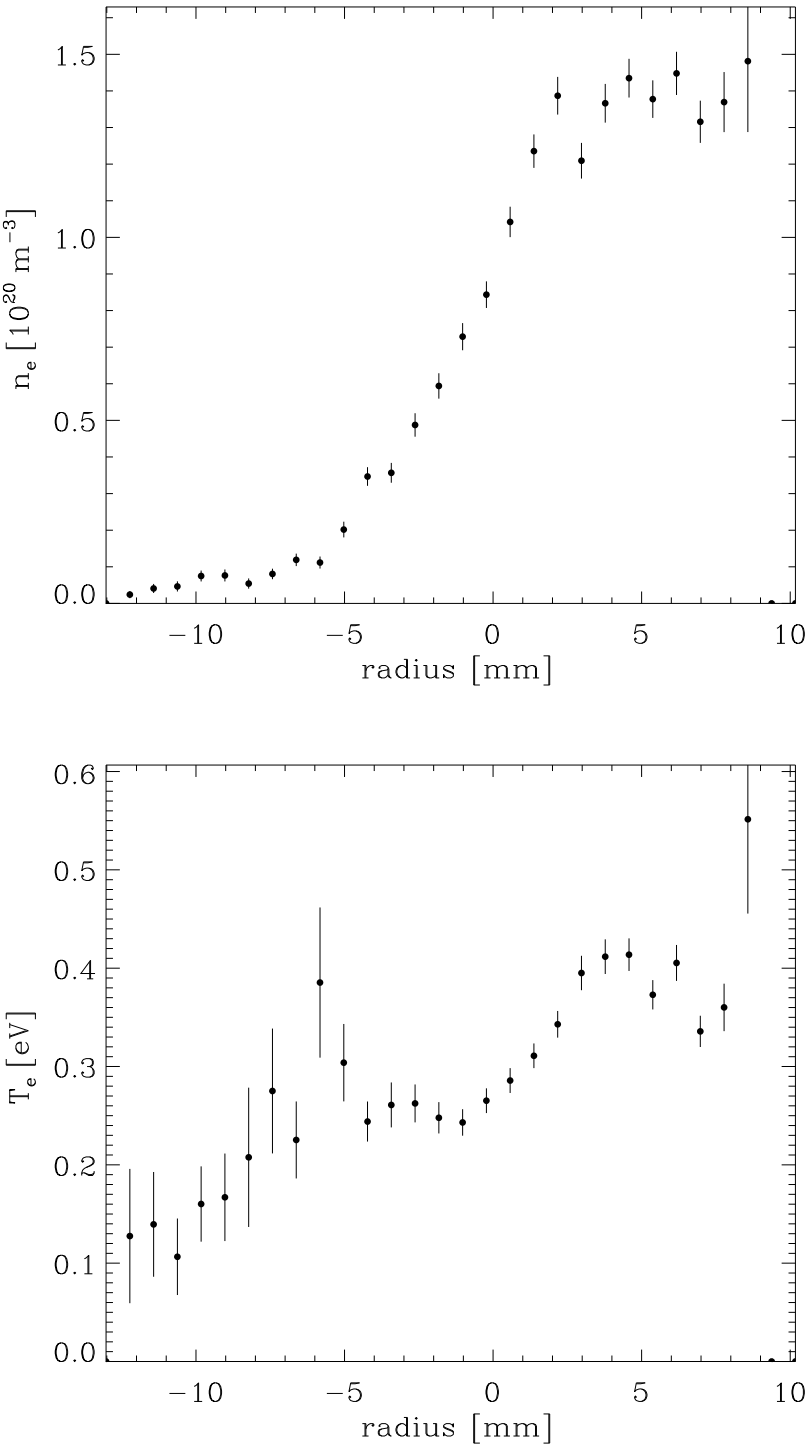

FIGURE 4.1: Typical TS profiles, i.e. electron density and temperature with respect to the lateral position. The center of the beam corresponds to the maximum values. While the profiles should be symmetric, i.e. Gaussian like, the other half is missing due to the position of the receiving fiber channels.

described in the previous chapter, and probe flux densities. An overestimation is found

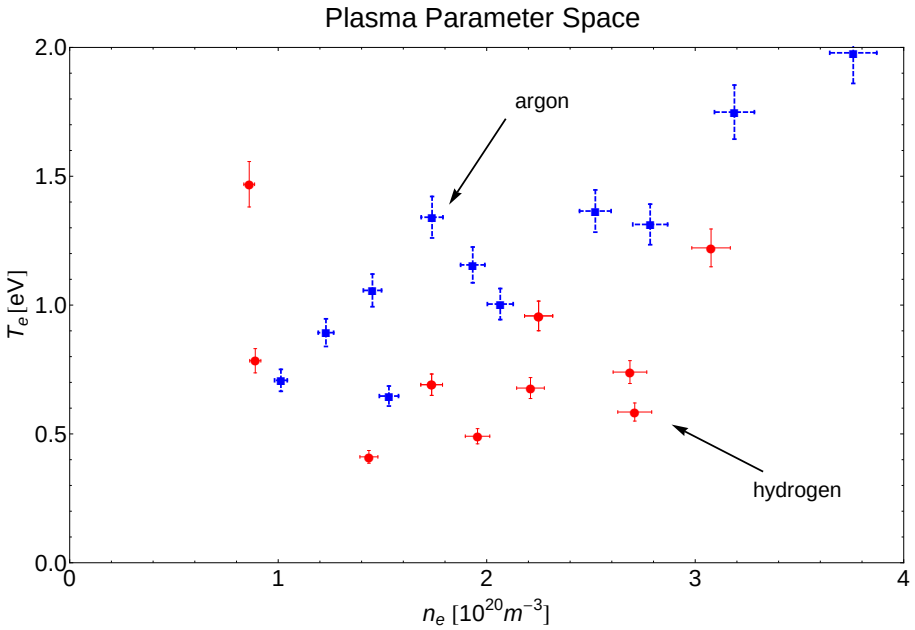

FIGURE 4.2: This figure shows combinations of H_2 and Ar plasma density and temperature that were evaluated in the present work corresponding to flux densities of $\approx 10^{24}\ m^{-2}s^{-1}$. The source current was varied from $125 - 200$ A with a flow of $1 - 3$ slm. The magnetic field ranged $0.4 - 1.2$ T.

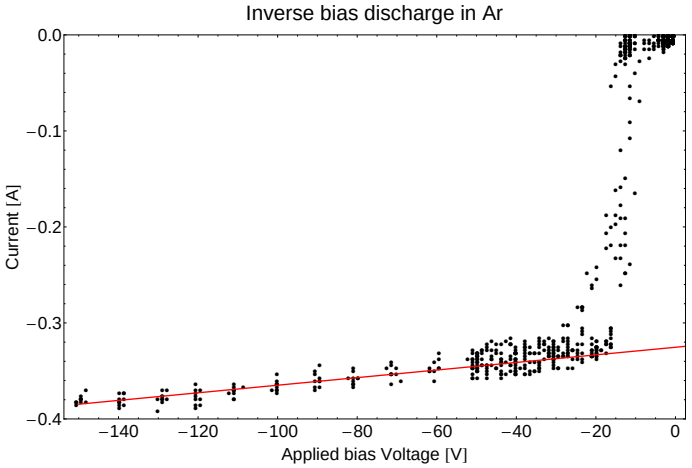

FIGURE 4.3: Typical I-V characteristic in hydrogen plasma. The source current was 200 A with a flow of 3 slm. The magnetic field was 0.4 T. Corresponding electron density and temperature are $\approx 2 \cdot 10^{20}$ m^3 and 0.5 eV respectively. $I_{sat} = -0.32$ A. Saturation current (extrapolated) provides direct measurement of the particle flux density at target.

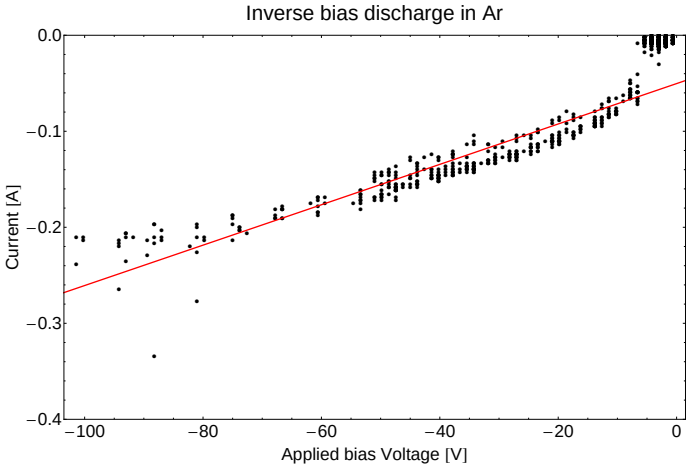

FIGURE 4.4: Typical I-V characteristic in argon plasma. The source current was 150 A with a flow of 1.5 slm. The magnetic field was 0.4 T. Corresponding electron density and temperature are $\approx 3 \cdot 10^{20}$ m^3 and 1.7 eV respectively. $I_{sat} = -0.05$ A. Saturation current (extrapolated) provides direct measurement of the particle flux density at target

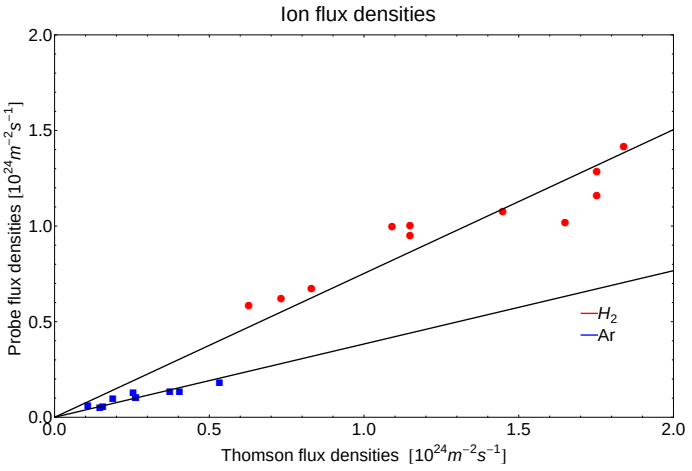

FIGURE 4.5: This figure shows ITER relevant flux densities for hydrogen plasma-red dots, and argon plasma-blue dots in Pilot-PSI. Comparison of flux densities from probe measurements with those from Thomson densities learns that assumption M=0.5 at the Thomson position (inspired by general sheath theory) is not valid.

when classical sheath theory is applied for computing these fluxes Equation 4.2.

$$\Gamma_{\text{Probe}} = 0.75\Gamma_{\text{Thomson}} \quad \text{in case of} \quad H_2 \tag{4.1}$$

$$\Gamma_{\text{Probe}} = 0.38\Gamma_{\text{Thomson}} \quad \text{in case of} \quad Ar \tag{4.2}$$

Under the assumption that the ion fluxes are conserved within the plasma beam, i.e. the upstream flux is the one that reaches the target and is detected with the Langmuir probe, target fluxes are related with upstream ones and Mach numbers are obtained, as is shown in Figure 4.6. These correspond to typical flow velocities at the Thomson position, of the order of 5000 m/s for hydrogen plasma and 500 m/s for argon plasma.

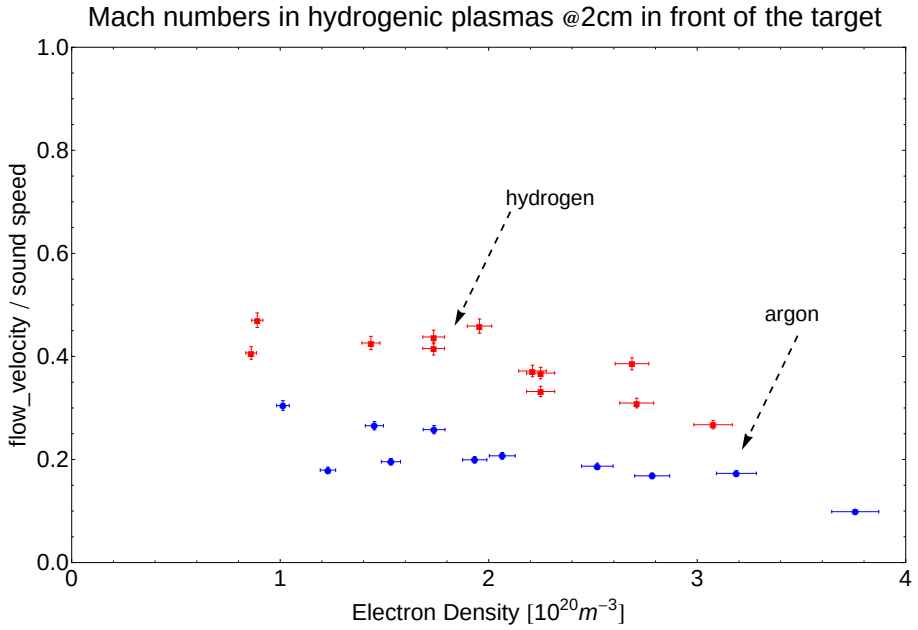

FIGURE 4.6: Mach number as a function of plasma density measured in Pilot-PSI. The Mach number slightly decreases with density probably due to changes in pre-sheath length. Flow velocities in H_2 are $\approx 5\ km/s$, an order of magnitude higher than in Ar.

An explanation for the slight decrease of Mach numbers with density is attempted. A first approach was discussed in [5] where the pre-sheath length was expanding beyond the Thomson measuring position thus making the upstream location a point with a higher plasma flow velocity Figure 4.7. A change in the pre-sheath length scale may be expected on the basis of the different T_e which translate into different energy values that the ions impinging on the target acquire over the sheath. Therefore, the neutrals will return with different velocities back into the plasma that can stop close to target or further away based on their collision frequency with ions in the plasma. In addition, this frequency depends also on the plasma density, i.e. the more dense the plasma, the larger will be the stoping power for the neutrals. Assuming the pre-sheath being determined by the neutrals, it can be that its length scale varies according to the parameter space in which the experiment was done.

Langmuir probe experiments together with Thomson scattering were performed on plasma column in both argon and hydrogen plasmas. Operation conditions were in the ITER relevant regime in terms of particle fluxes and heat fluxes. Classical sheath theory, yields an over estimation of particle fluxes towards the target is found within a factor of 1.3 to 2.6 for H_2 and Ar with respect to the Langmuir probe results.
In addition, Mach numbers of 0.2 for argon and 0.5 for hydrogen were determined as well together with their corresponding flow velocities. A preliminary explanation involving pre-sheath length expansion was used in order to acquaint the slight increase of Mach numbers with declining density. The applicability of the "classical sheath" theory

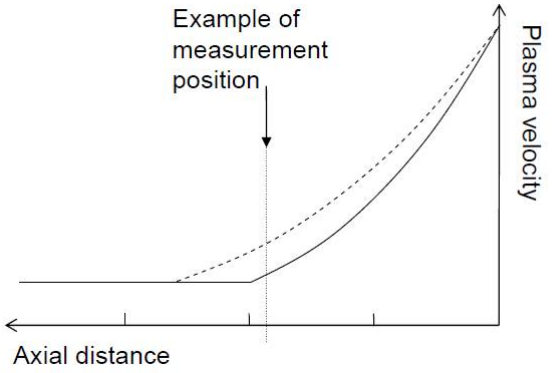

FIGURE 4.7: This figure shows how an increasing pre-sheath length can affect the measurement of the plasma flow velocity. Basically, an already accelerated plasma is measured if the pre-sheath expands beyond the detection point.

is rather limited in the present context where plasma convection and plasma neutral interaction are expected to play a dominant role.

Chapter 5

One fluid plasma model

5.1 Introduction

In this chapter the the one fluid model of the plasma is introduced together with the neutral model. This model incorporates elements that allow for a further benchmark with the results from experiments. Stationary plasma profiles along the magnetic field lines, that is, within the so-called flux tube constitute the solutions of the model. The equations underlying the model differ from other approaches used in literature, e.g. [14], [10], in the way the neutral atoms interact with the plasma, e.g. the possibility of heating up the plasma via charge exchange processes. This is due to the fact that the high plasma density in Pilot-PSI ensures that the heat of the neutrals is effectively captured while in tokamak conditions electron temperatures are generally much higher and there the recycling of the particles can cause already a significant portion of the heat to be captured.

5.2 System of equations

A simple 1D geometrical approach is used for the model. The spatial variable along the magnetic field line is denoted by x and the origin of the system, $x_0 = 0$, is chosen at the sheath entrance (se). The end point, x_1 is in the order of tens of cm where no spatial changes are observed anymore in the simulated profiles. The Bohm criterion is taken as a boundary condition at the sheath entrance. In addition, everywhere in the integration domain, the plasma is current free, i.e. $v_e = v_i = v$, and quasineutral, i.e. $n_e = n_i = n$. Moreover, as a starting point coupling between electron and ion temperature is assumed, $T_e = T_i = T$. Stangeby argues in the documentation of the impurity code DIVIMP [15] that interpretative modeling is best done in the upstream

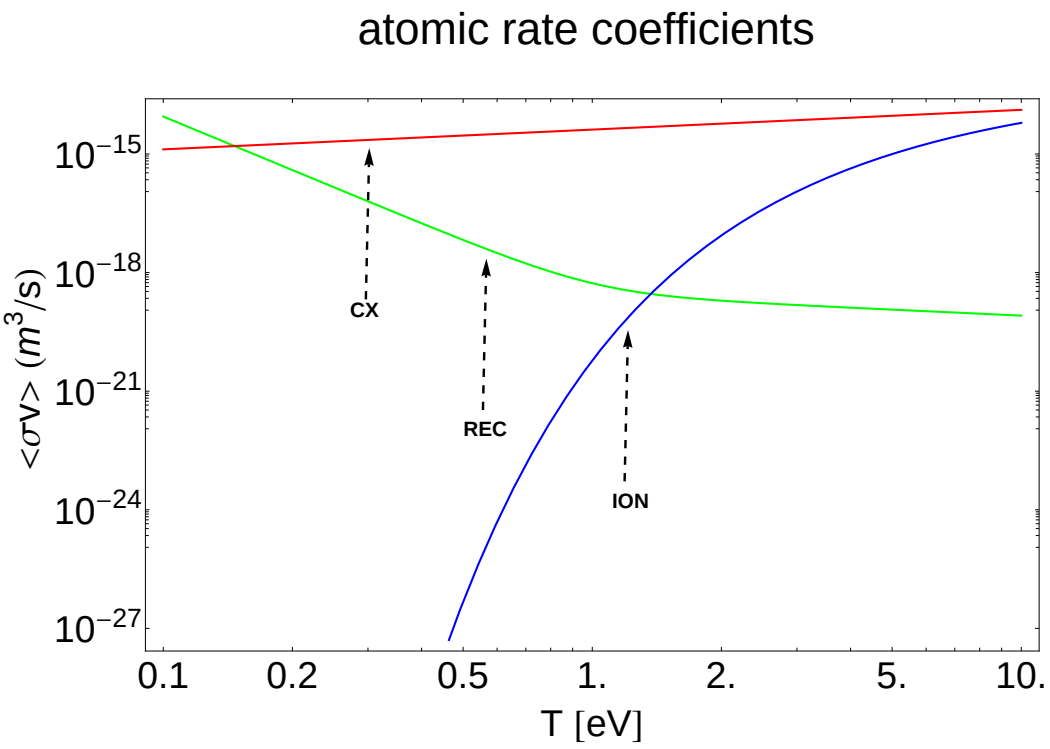

FIGURE 5.1: Atomic rate coefficients for hydrogen where CX stands for charge exchange processes, REC for recombination and ION for ionization.

direction starting from the target region. Among his arguments, stability of the target boundary conditions in opposition with the volatility character of the upstream ones was critical for the approach taken in present work. However, upstream modeling has its limitations, that will be shown at a later stage in this project.

The plasma consists of hydrogen ions, electrons and neutral hydrogen atoms with the following atomic processes taken into consideration:

$$\begin{aligned} &(CX)\ H + H^+ \rightarrow H^+ + H \\ &(ION)\ H + e^- \rightarrow H^+ + 2e^- \\ &(REC)\ H^+ + 2e^- \rightarrow H + e^-. \end{aligned} \tag{5.1}$$

Here CX, ION and REC stand for charge exchange, ionization and recombination, respectively with their reaction rates are functions of energy and plotted in Figure 5.1.

The fluid equations represent the different moments of the Boltzmann distribution function of electrons and ions together with an appropriate closure scheme. They have been

already derived by Braginskii in 1965 [16].

$$\begin{aligned}
&\frac{d}{dx}(nv) = S_1 \\
&\frac{d}{dx}(m_i n v^2 + 2nT) = S_2 \\
&\frac{d}{dx}(m_i \frac{1}{2} n v^3 + 5nvT - k_\parallel \frac{dT}{dx}) = S_3
\end{aligned} \tag{5.2}$$

The right hand side of the plasma equations represent the plasma sources and sinks due to ionization, recombination and charge exchange :

$$\begin{aligned}
&S_1 = k_{\text{ion}} n n_n - k_{\text{rec}} n^2 \\
&S_2 = m(v_n - v) K_{\text{cx}} n n_n - mv K_{\text{rec}} n^2 \\
&S_3 = -K_{\text{ion}} n n_n E_{\text{ion}} - K_{\text{rec}} n^2 (\frac{1}{2} m_i v^2 + 3T) + K_{\text{cx}} n n_n (E_{\text{refl}} - (\frac{1}{2} m_i v^2 + \frac{3}{2} T)).
\end{aligned} \tag{5.3}$$

The first term in S_1 represents the ionization of neutrals recycled from the target plate and the second one gives the loss of particle at low temperature due to recombination. The ion momentum term S_2 includes only losses due to recombination and friction with neutrals via charge exchange. Finally, the energy term S_3 includes energy losses due to ionization, recombination and an energy gain due to charge exchange .

The neutrals are a key element in the previous equations due to their presence as a source and sink in both momentum and energy equations. Basically, there is a monoenergetic population of neutrals which comes back from the target into the plasma where the CX process throws them away. This yields the following equation 5.4 for the neutrals:

$$v_{\text{n}} \frac{dn_n}{dx} = -K_{\text{cx}} n_{\text{n}} n \tag{5.4}$$

where $v_n \approx \sqrt{2E_{\text{refl}}/m_{\text{ion}}}$. In addition, $v_n n_n = R_N c_s n$ and $E_{\text{refl}} = R_E(2T_i + 3T_e)$, where R_N and R_E are particle and energy reflection coefficients, respectively. Stangeby, takes for the ion energy flux that reaches the solid surface the $q^i_{\text{ss}} = (2T_i + |eV_{\text{sh}}|)\Gamma_{\text{se}}$, which under the assumption of temperature equilibrium between ions and electrons, floating target and a reflection coefficient $R_E = 0.6$ for hydrogen on tungsten, gives a reflected energy $E_{\text{refl}} = 3T$ back into the plasma [10]. It is worth noticing already at this point the important distinction between the floating and biased cases that can have a radical influence on the energy of the neutrals reflected back into the plasma.

Furthermore, the neutral velocity appears in the momentum equation as well, contributing to the friction term and inherently to plasma acceleration as it is going to be shown in the coming chapter. Moreover, the neutrals are explicitly giving their energy via CX processes to the ions which should lead to a temperature imbalance between ions and electrons. A quantization of this effect is addressed in a separate section as well by equating the charge exchange energy gain with the energy equilibration term in between ions and electrons.

In order to reduce the system of equations 5.2 to a first order degree of differential equations and to simplify it the following changes are made:

$$\begin{aligned} C_1 &= nv \\ C_2 &= m_i n v^2 + 2nT \\ C_3 &= m_i \frac{1}{2} n v^3 + 5nvT - k_{\parallel} \frac{dT}{dx}. \end{aligned} \tag{5.5}$$

Here $k_{\parallel} \approx 4000 T^{5/2}$ is the parallel electron conduction of the plasma, C_1, C_2 and C_3 are particle flux, momentum flux and heat flux, respectively.

The complete set of fluid equations are rewritten with these new set of variables as follows:

$$\begin{aligned} &\frac{d}{dx} C_1 = K_{\text{ion}} n n_n - K_{\text{rec}} n^2 \\ &\frac{d}{dx} C_2 = m(v_n - v) K_{\text{cx}} n n_n - m v K_{\text{rec}} n^2 \\ &\frac{d}{dx} C_3 == -K_{\text{ion}} n n_n E_{\text{ion}} - K_{\text{rec}} n^2 (\frac{1}{2} m_i v^2 + 3T) - K_{\text{cx}} n n_n (\frac{1}{2} m_i v^2 + \frac{3}{2} T) + K_{\text{cx}} n n_n E_{\text{refl}} \\ &\frac{dT}{dx} = -\frac{1}{k_{\parallel}} (C_3 - (m_i \frac{1}{2} n v^3 + 5nvT)). \end{aligned} \tag{5.6}$$

The new set of equations contains plasma density and velocity in the right hand side and their values need to be back up from the notation that we made in equations 5.5. Starting from the particle flux C_1 and momentum flux C_2 one can solve the second degree equations for the density and get two solutions :

$$n = \frac{C_2 \pm \sqrt{{C_2}^2 - 8 m_i {C_1}^2 T}}{4T} \tag{5.7}$$

The positive branch of the density solution is chosen. An explanation follows:

We analyze the terms under the square root $\sqrt{C_2^2 - 8mTC_1^2}$:
i) $C_2 = mnv^2 + 2nT = mn(v^2 + c_s^2) \Rightarrow C_2^2 = m^2n^2(v^2 + c_s^2)^2$
ii) $8mTC_1^2 = 8mn^2v^2 = 4m^2n^2v^2c_s^2$
We have made use of the fact that $c_s = \sqrt{\frac{2T}{m_i}}$. The difference under the square root can be written as perfect square:
$C_2^2 - 8mTC_1^2 = m^2n^2(v^4 - 2v^2c_s^2 + c_s^4) = m^2n^2(v^2 - c_s^2)^2$
Therefore, taking the square root imposes a modulus around the remaining value:
$\sqrt{C_2^2 - 8mTC_1^2} = mn|v^2 - c_s^2|$.

As a result the density equation 5.7 becomes:

$$n = \frac{mn(v^2 + c_s^2) \pm mn|v^2 - c_s^2|}{2mc_s^2}. \tag{5.8}$$

We have not measured supersonic velocities therefore we expect to be in a subsonic regime where plasma velocity is less than sound speed: $v < c_s$. Under this condition the density equation, after resolving the modulus, becomes :

$$n = \frac{mn(v^2 + c_s^2) \pm mn(c_s^2 - v^2)}{2mc_s^2}. \tag{5.9}$$

With the two branches explicitly :

$$n_+ = n \tag{5.10}$$
$$n_- = n\frac{v^2}{c_s^2} \tag{5.11}$$

Therefore, the choice for the + sign in order to recover the initial input density value in the definition of C_1 and C_2. A sonic transition would require a change in branches.

5.3 Quantification of T_i increase due to CX heating

In order to get an idea of the maximal difference between the ion temperature and the electron temperature, we equate the power that neutrals deposit locally into the plasma to the power exchange between electrons and ions:

$$K_{\text{cx}}n_nn(E_{\text{refl}} - (\frac{3}{2}T_i + \frac{1}{2}m_iv^2)) = \frac{3m_en}{m_i}\nu_{\text{eq}}(T_i - T_e) \tag{5.12}$$

For a more compact form, the same equation can be rewritten as the ratio between the relative temperature increase to the difference in kinetic energy between the neutrals

and the ions:

$$\frac{\Delta T}{\Delta E} = \frac{K_{\mathrm{cx}} n_n}{\frac{3m_e}{m_i}\nu_{\mathrm{eq}}} \tag{5.13}$$

5.4 Boundary conditions

The system of plasma fluid equations together with the model describing the neutrals is integrated from the target towards the upstream as an initial value problem, i.e. boundary conditions are given only at one point: the sheath entrance, as it is shown schematically in Figure 5.2. The following two parameters are fixed at the point x_0 : density n_0 and temperature T_0. The Bohm criterion states that the ions enter the sheath with sound velocity $c_{\mathrm{s0}} = \sqrt{\frac{2T_0}{m_i}}$. Having these established, starting values for particle, momentum and energy fluxes are computed according to equation 5.5. In addition, the initial conduction heat flux $\mathrm{Q}_{\mathrm{cond}}$ is null since we are mainly interested in a convective flow regime similar to that of the PILOT-PSI plasma regime.

FIGURE 5.2: Schematic ilustration of the 1D 'mesh'.

Chapter 6

1D, 1-fluid modeling of the effect of the neutral source

This chapter contains the results obtained with the numerical model outlined in the previous chapter. First, the effect of high energetic neutrals in the energy balance is investigated. After that the influence of target biasing and the energy reflection coefficient is assessed. Subsequently, the simulated flow profiles are compared with the measured flow velocities of chapter 4. A limit case of the model corresponding to thermal neutrals is investigated as well. Finally, the effect on target heat loads are addressed as well as argon plasma behavior.

6.1 The effect of high energetic backscattered neutrals in the energy balance

We investigate the effect of energy exchange with the neutrals in the energy balance by comparing two cases. In the first case, which we will refer to as "CX on" we solve the system of equations as outlined before (eq. 5.6). The second case we will refer to as " CX off" and consisted of setting $E_{refl} = 0$ in the charge exchange term of the energy balance (eq. 5.6) whilst keeping $v_n = \sqrt{2E_{refl}/m}$ in the momentum equation. Figure 6.1 shows the modeling results. The target conditions, namely the boundary conditions for the ODE system, were varied for the two distinct cases in order to match the same upstream profiles in terms of temperature and particle flux (which also means heat flux in the low temperature convective regime) and have this as a basis for comparison. An additional reasoning for matching upstream this profiles comes from the experimental situation in which an upstream plasma source delivers a set particle and energy flux.

It is seen that the particle flux is hardly changing along the axial distance. This is due to low ionization and recombination rates in this energy interval.

The momentum flux profiles are different in the two situations: with CX energy off, there is less friction with the neutrals and therefore there is less build up of momentum in the upstream region as opposed to the case when CX energy is on. This is due to a different neutral velocity in the two cases, i.e the neutrals have a higher velocity when CX energy is on. The neutrals are monoenergetic and have an energy proportional to the sheath energy. In turn, this sheath energy (for a floating wall) is proportional to the plasma temperature and we do see an increase of plasma temperature near the target when CX energy is on. Another behavior of the faster neutrals is that they penetrate further into the plasma and this can be seen in the distance over which the momentum flux builds up as well as in the neutrals' profile themselves.

The density profiles are derived from the momentum and particle fluxes as explained in the previous chapter. Since the particle flux is constant what makes a difference in the density profile is the momentum flux. The density profiles follow the behavior of the momentum flux profiles.

The Mach number is, since the particle flux is constant, simply proportional to the inverse of the density profile. However, it is relevant to discuss it from the point of view of a plasma acceleration. Already more than two decades ago Riemann underlined this mechanism in his review paper on Sheath Physics [12]. In order for the Bohm criterion to be satisfied, an acceleration region of quasineutral plasma must exist for this to happen. In literature, this acceleration zone is conventionally named pre-sheath. In a collisional

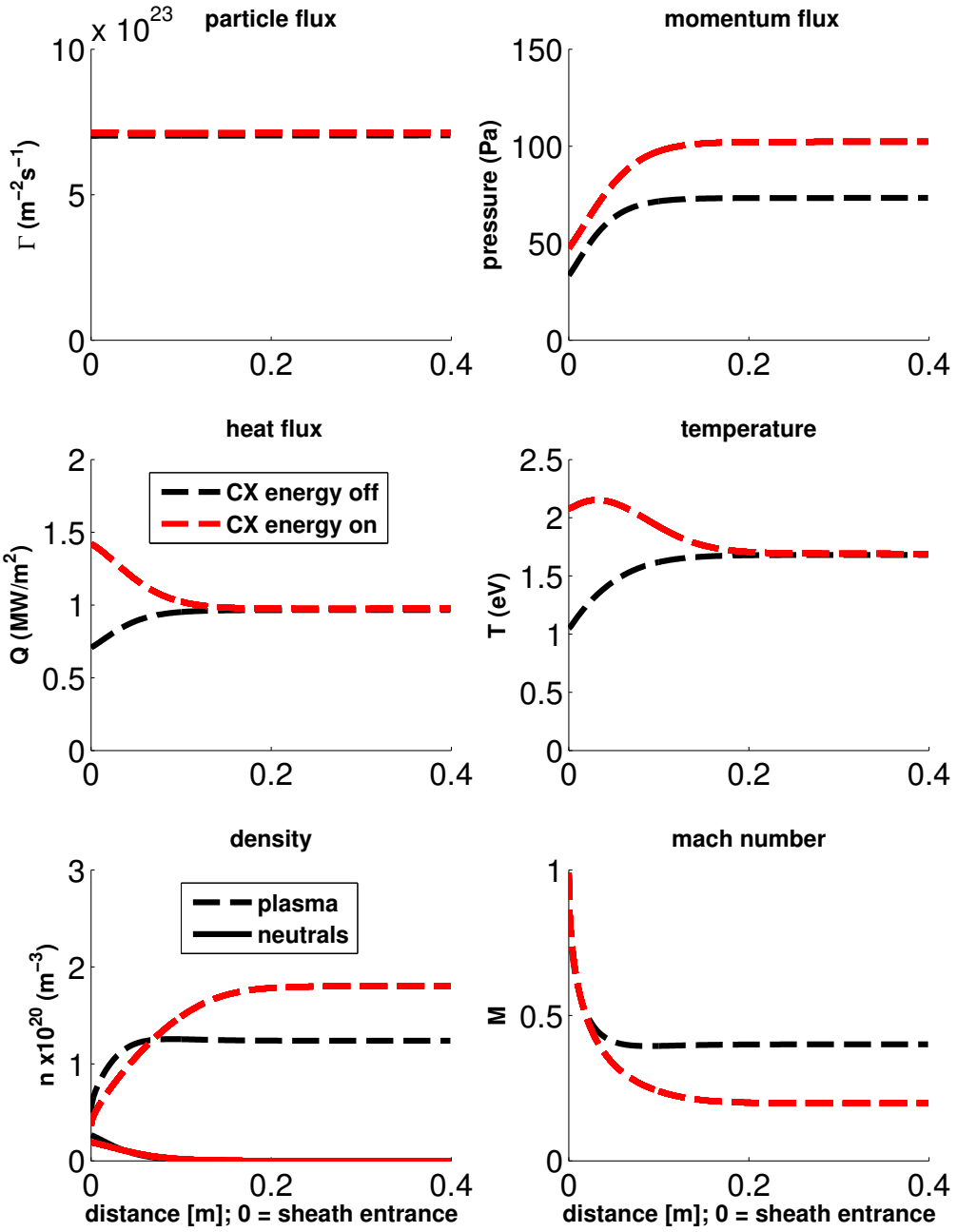

FIGURE 6.1: Near wall plasma heating from backscattered neutrals. Starting conditions: $n_0 = [5, 3.6] \times 10^{19}\ m^{-3}, T_0 = [1.05, 2.08]\ eV, R_E = 0.7, R_N = 1$. In the first case, black profiles, the neutrals are mainly responsible for removal of momentum from the plasma and as a result the plasma cools down due to convection. In the other case, active heating of the plasma show an almost two times increase in both plasma edge temperature and heat flux.

plasma the neutrals create a drag force on the ions removing momentum from the plasma. This removal of momentum leads to a pressure build up in the upstream region of the plasma which subsequently is responsible for the force providing the acceleration. An important aspect here is the match of this acceleration length with the neutral penetration depth which is subsequently determined by the neutrals' initial velocity. Another aspect relates to the plasma acceleration due to friction as we see in this profiles. Imagine the neutral density becomes zero, then most of the sources and sinks would become negligible. This means that the plasma remains sonic all over the simulated space. To conclude on this aspect, we regard the length scale over which the plasma accelerates to sound speed as the pre-sheath. However, we note that effects like non-Maxwellian distribution and finite electric fields that also must be present are not taken into account by the model.

The effect of plasma heating by the neutrals is most evident in the profiles of temperature and heat flux. Without heating, the plasma looses energy in the charge exchange with neutrals so that both profiles drop towards the target. Taking the larger energy for the neutrals into account gives the opposite.

The leveling off of heating in the last cm's in front of the target is due to the acceleration of the plasma. The convected energy is $(\frac{1}{2}m_i n v^3 + 5nvT)$, and when the plasma goes from $\approx 0.5c_s$ to c_s this has to be compensated by a drop in T if no additional energy is conducted.

Having established that the heating effect is significant, we ask ourselves the question whether $T_e = T_i$. The reason for this question is Shumack's work [5], in which no temperature increases were found in the electrons and it was postulated that only the ions were heated. In order to get an insight into the maximum increase of the ion temperature relative to the electron temperature, a balance between the ion surplus of energy due to CX collisions with hot neutrals and the electron-ion energy equilibration term is considered. The result is shown in Figure 6.2 as was calculated for the simulation results in Figure 6.1. We see that at floating target conditions there is a maximum increase of ≈ 0.8 eV that extend up to ~ 10 cm into the plasma.

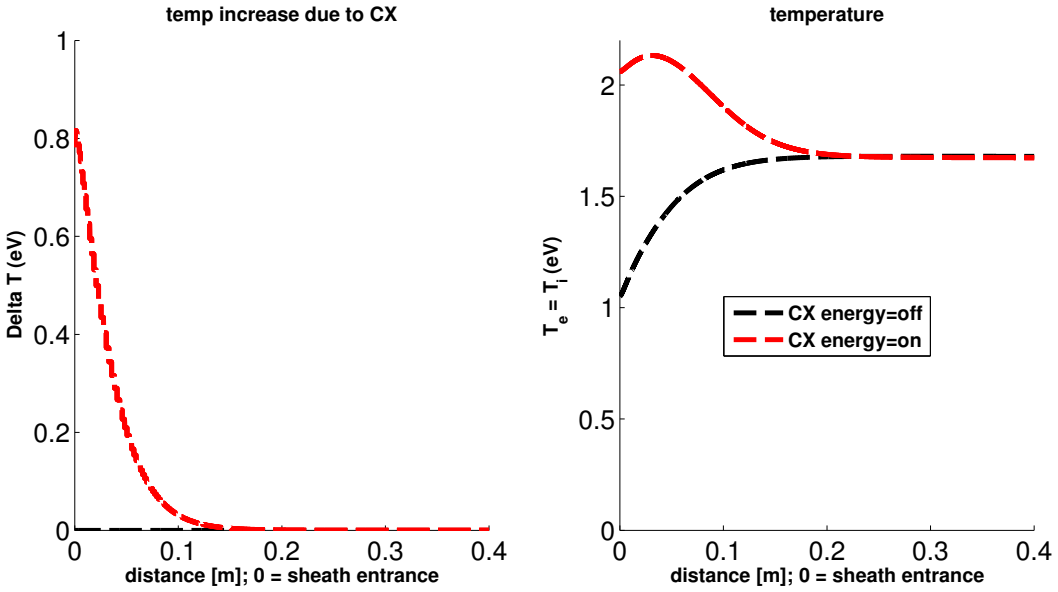

FIGURE 6.2: Relative increase of T_i under heating from backscattered neutrals. Starting conditions: $n_0 = [5, 3.6] \times 10^{19}\ m^{-3}, T_0 = [1.05, 2.08]\ eV, R_E = 0.7, R_N = 1$.

6.2 Target biasing: how an experimental tool in PSI research dictates upstream conditions

In this section we evaluate the heating for biased targets. Target biasing obviously gives much more energy to the neutrals compared to floating targets and it is a common procedure to vary the ion impact energy in plasma surface experiments. The ion energy near the target has one component proportional with the sheath voltage ($2T_i + |eV_{\mathrm{sh}}|$), which for a floating case is $\approx 3T_e$.

Simulated plasma profiles for two different bias voltages are compared with the floating situation in Figure 6.3. Again, the approach was matching of the upstream plasma conditions in terms of temperature, particle flux and heat flux by iterating the boundary conditions at the target. The maximum possible difference between ion and electron temperature calculated from these profiles is shown in Figure 6.4. The increase in plasma temperature near the target with respect to the upstream temperature was evaluated as a function of the applied target bias and plotted in Figure 6.5 .

The plasma temperature together with the heat flux increase near target as a result of input energy from the backscattered neutrals under biasing conditions. Having as a reference the same temperature and energy flux in the upstream region it is clearly seen that the higher the bias or the energy input, the higher the temperature increase. However, during the entire bias sweep the energy reflection coefficient R_E was kept constant and this is not entirely true in reality as there is a variation as a function of the impact energy. We note that the comparison of the present 1D modeling with experimental values in terms of the length scale of the pre-sheath comes into question. Once it exceeds plasma diameter, particle escape will become important in a 2D geometry.

The pre-sheath length is observed to increase with biasing. The more energy the neutrals have, the further they penetrate into the plasma before undergoing charge exchange. The results are a clear confirmation that biasing induces acceleration and rarefication near the target. This brings up a concern for the common practice at Pilot-PSI to deduce plasma flux densities from Thomson scattering at a fixed position close to the target assuming a constant plasma velocity. The present simulations show that changes in the pre-sheath length scale complicate this practice.

Equating the CX energy input with the equilibration term shows the proportional increase of ion temperature with biasing. It is instructive at this point to do the following exercise: Say all energy input from the neutrals goes to the ions while the electrons remain at the same upstream plasma temperature. Taking the -20 V bias case in Fig. 6.4, ions would have a temperature of $\approx 7\ eV$ at the target. Averaged with the 1 eV of

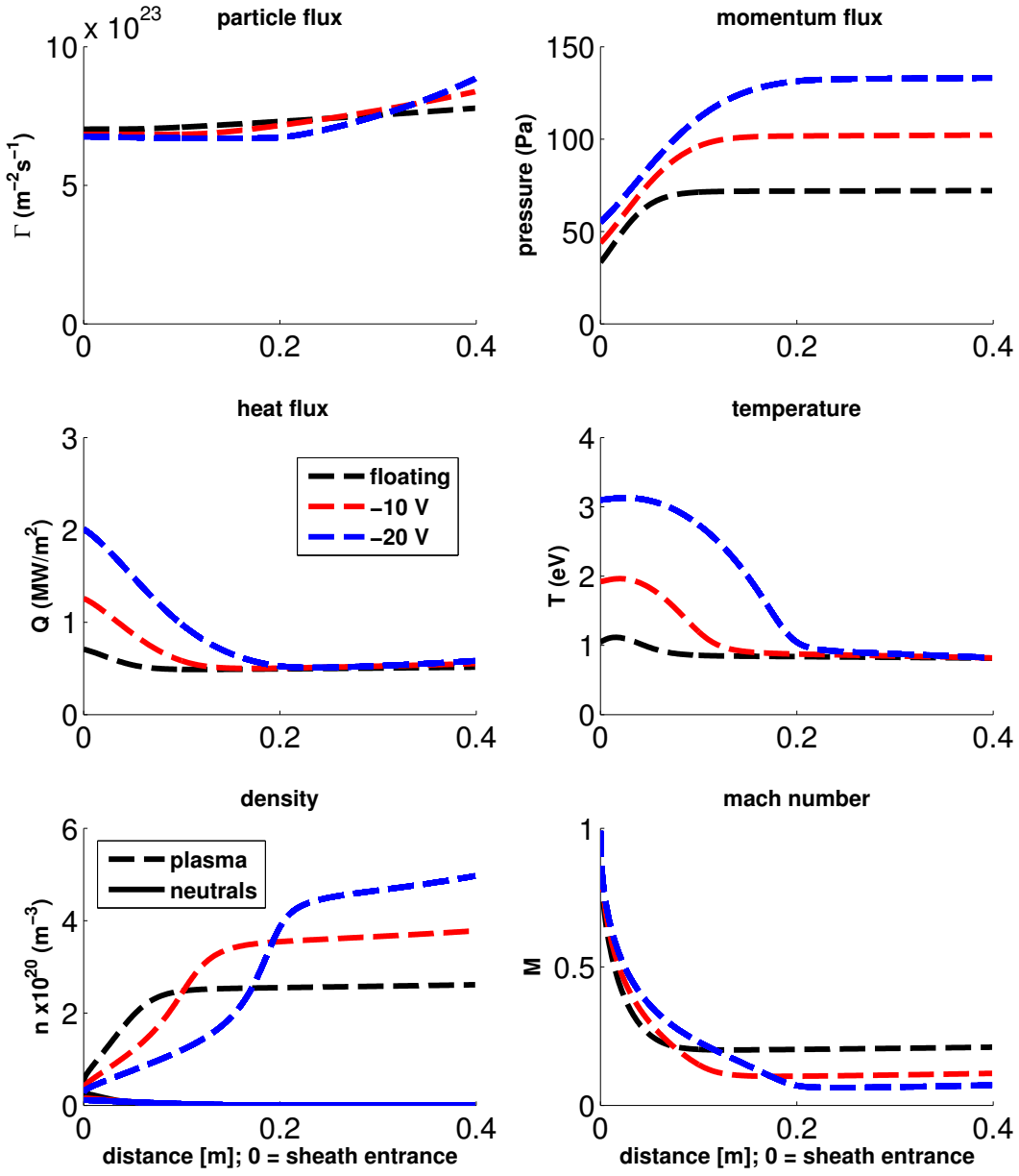

FIGURE 6.3: Plasma profiles under a negative bias scan. Starting conditions: $n_0 = [5, 3.6, 2.8] \times 10^{19}\ m^{-3}, T_0 = [1.05, 1.92, 3.1]\ eV, R_E = 0.7, R_N = 1.$

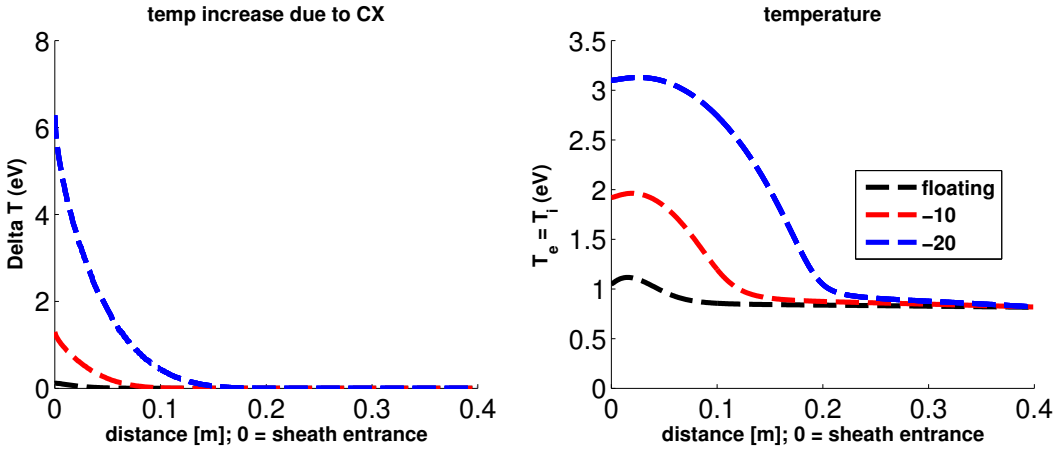

FIGURE 6.4: Relative increase of T_i under a negative bias scan. Starting conditions: $n_0 = [5, 3.6, 2.8] \times 10^{19}\ m^{-3}, T_0 = [1.05, 1.92, 3.1]\ eV, R_E = 0.7, R_N = 1.$

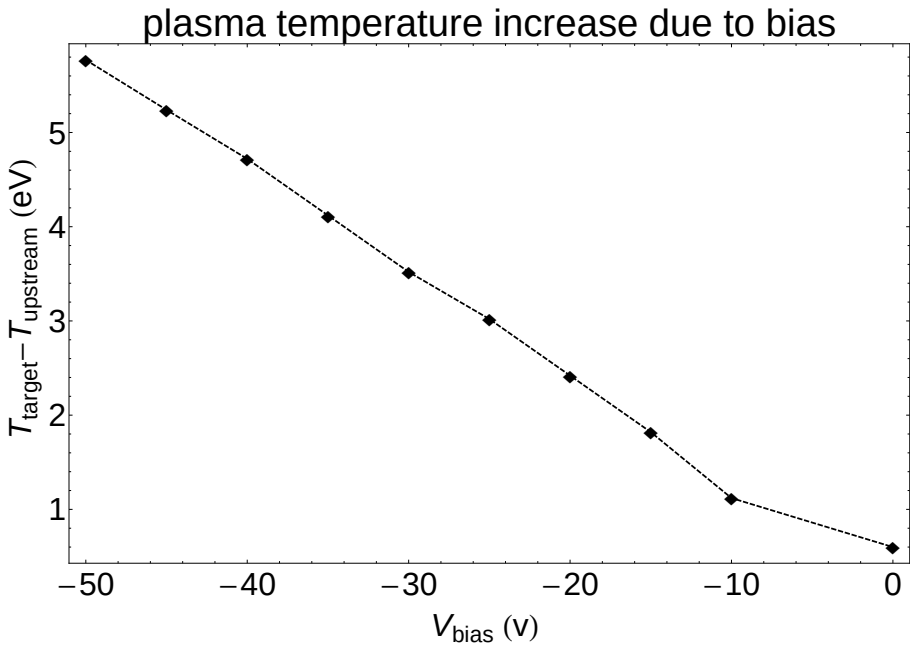

FIGURE 6.5: In this picture the near wall plasma temperature increase with respect to the upstream plasma temperature due to target biasing. Technically, the target is at a negative floating potential of $\sim -3V$ even without bias and a shift to the left should be taken into consideration.

the electrons this would give 4 eV plasma temperature at the target, whereas the 1 fluid model predicts $\sim$ 3 eV. We thus conclude that a temperature inequilibrium of a few eV is well possible in this situation, which supports the earlier estimates of Shumack.

6.3 An energy reflection coefficient scan, R_E

In this section the energy reflection coefficient R_E is varied. For the sake of simplicity a target floating case is considered. Results of the plasma profiles are presented Figure 6.6. A relative increase of target plasma temperature with respect to upstream plasma due energy reflection coefficient is shown in Figure 6.7. In addition, a relative increase of ion temperature with respect to electron temperature due to energy reflection coefficient in shown in Figure 6.8.

From a simulation point of view, R_E is just another parameter for varying the energy that goes back into the plasma via the neutrals, i.e. similar to the applied voltage on the target. In reality, a different R_E is attributed to different materials and thus is worth investigating the effects of this scan.

Similar to the rationale in the biasing cases from the previous sections we matched the upstream profiles and looked for the effects at the target. An interesting result, encountered previously when CX energy was off, is the decreasing of plasma temperature at the target under the upstream value for a lower R_E. This means that no heating is provided anymore from the neutrals and the entire RHS of the plasma energy equation is dominated by the losses. A threshold value for R_E where heating starts to take place appear to be around $R_E \sim 0.6$.

The same effect is obtained when explicitly computing the relative difference of ion to electron temperature according to equation 5.12 due to the CX energy input. It appears that for lower energy reflection coefficients the transfer of energy from neutrals to plasma is negative, that is, the ions loose more energy to the neutrals than gaining from these ones. By increasing the R_E, several stages of this energy exchange are visible. It is worth noticing the mixed situations in which up to a point the energy transfer is ion favorable, the increasing part of the red line as viewed from the upstream, after which it turns into neutral favorable.

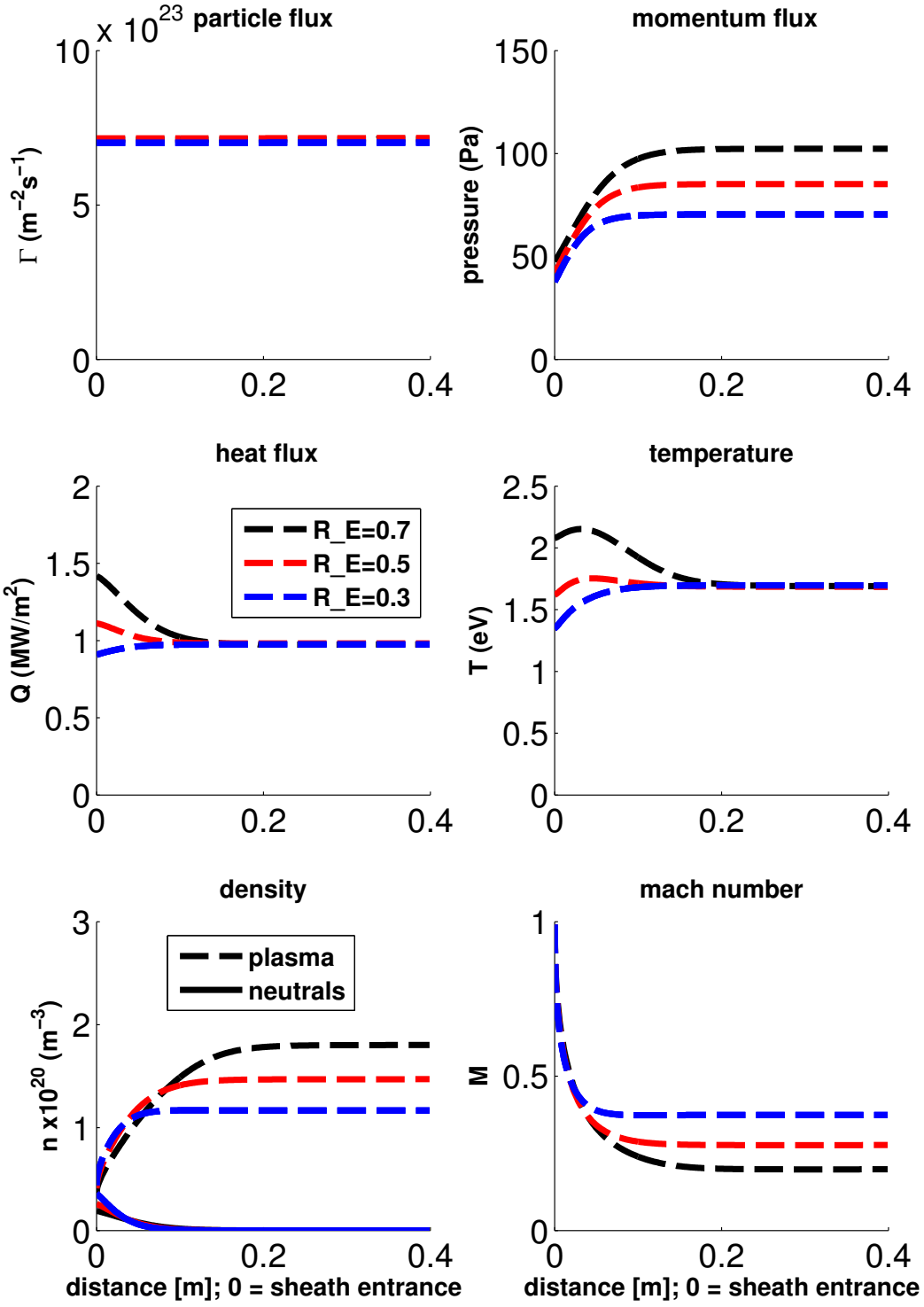

FIGURE 6.6: Plasma profiles under energy reflection scan scan. Starting conditions: $n_0 = [3.6, 4.1, 4.4] \times 10^{19}\ m^{-3}, T_0 = [2.08, 1.62, 1.35]\ eV, R_N = 1$.

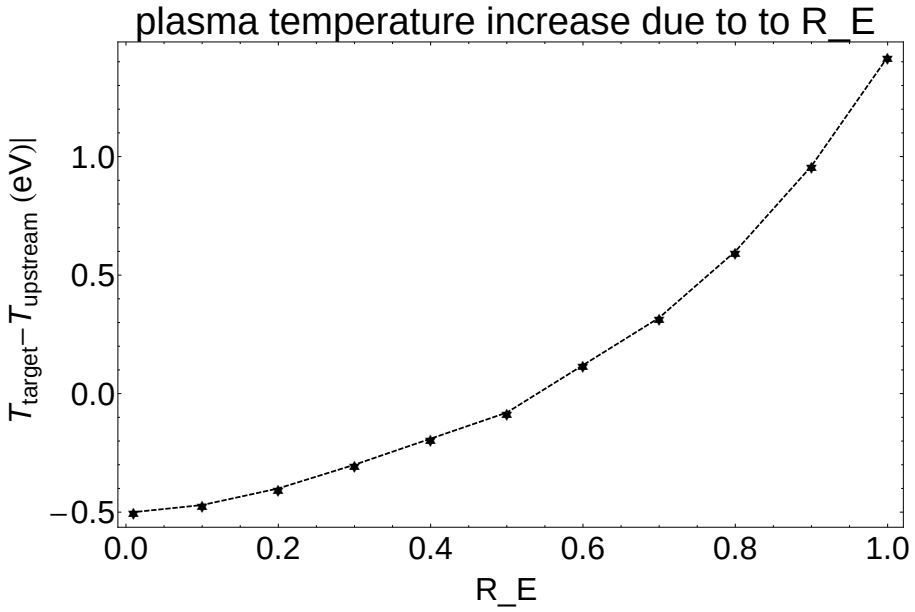

FIGURE 6.7: In this picture the near wall plasma temperature increase with respect to the upstream plasma temperature due to the reflection coefficient R_E.

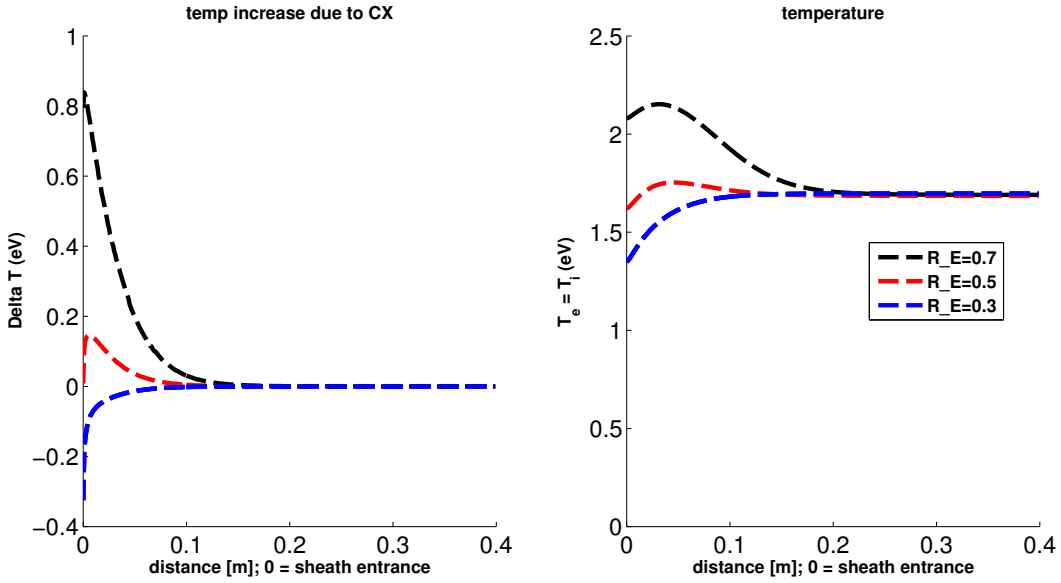

FIGURE 6.8: Relative increase of T_i under energy reflection scan. Starting conditions: $n_0 = [3.6, 4.1, 4.4] \times 10^{19}\ m^{-3}, T_0 = [2.08, 1.62, 1.35]\ eV, R_N = 1$.

6.4 Comparing simulated and measured flow velocities

The experimentally determined flow velocities were obtained at a distance of 2 cm in front of the target. We compare these with simulated Mach numbers at the same distance from the target in a sensitivity scan of the plasma parameters n_e and T_e and the material parameter R_E. The results are plotted in Figure 6.9. Simulations performed in a scan of the density are shown in Figure 6.10.

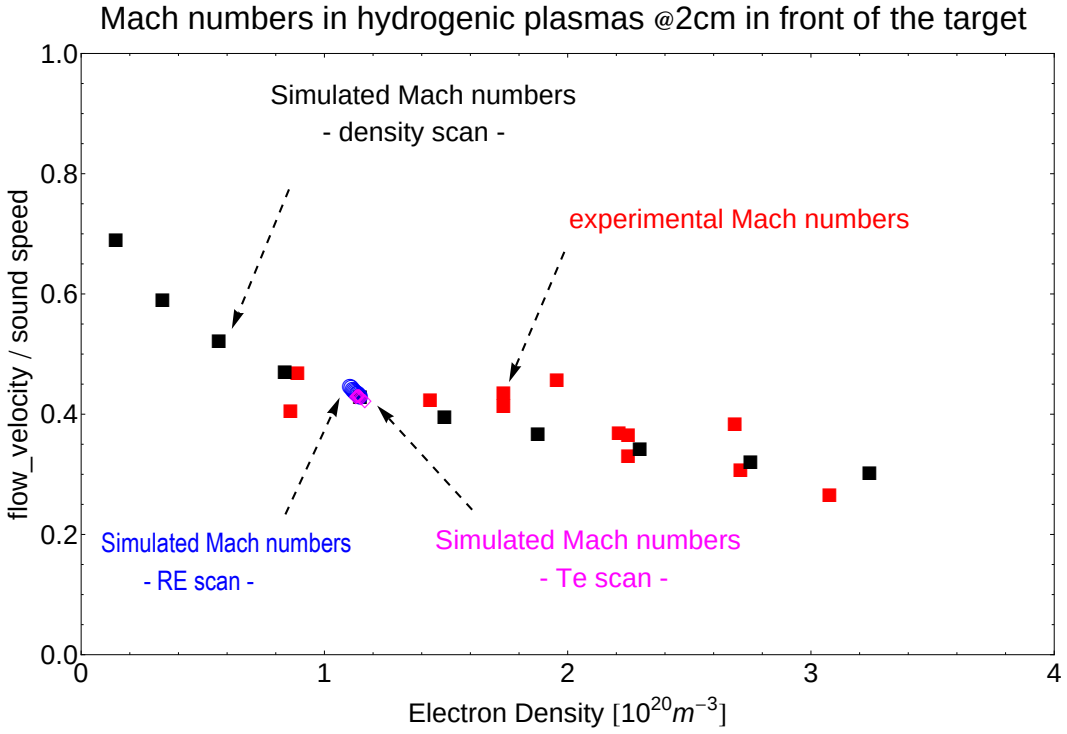

FIGURE 6.9: Mach numbers from experiment measurements with a Langmuir probe and from Simulations @2 cm in front of the target. Starting conditions for the simulations: $n_0 = (1:1:10) \times 10^{19}\ m^{-3}, T_0 = 2\ eV, R_E = 0.8$; $n_0 = 5 \times 10^{19}\ m^{-3}, T_0 = (1:0.5:5)\ eV, R_E = 0.8$; $n_0 = 5 \times 10^{19}\ m^{-3}, T_0 = 2\ eV, R_E = (0.3:0.05:0.8)$. A variation in initial density at the target shows the largest spread in terms of Mach number simulated range. The other two scans in T_e and R_E show hardly any variation of the Mach number for the current resolution. Overall, a good overlap in between measured values and simulation is observed.

The largest variation of the Mach numbers corresponds to a density parameter scan. This means friction has a determinant role into the plasma. Fewer particles means less friction for the neutrals that can set in deeper into the plasma. However, realistic dimensions of the plasma diameter need to be taken into consideration since at some point, the neutrals can simply escape from the plasma and therefore, no friction nor energy are provided anymore.

The plasma temperature appears to have hardly any influence on the Mach number at 2 cm in front of the target; a variation in the energy reflection coefficient gives a significant but still small expansion in the blue area. This is a consistent behavior that appeared

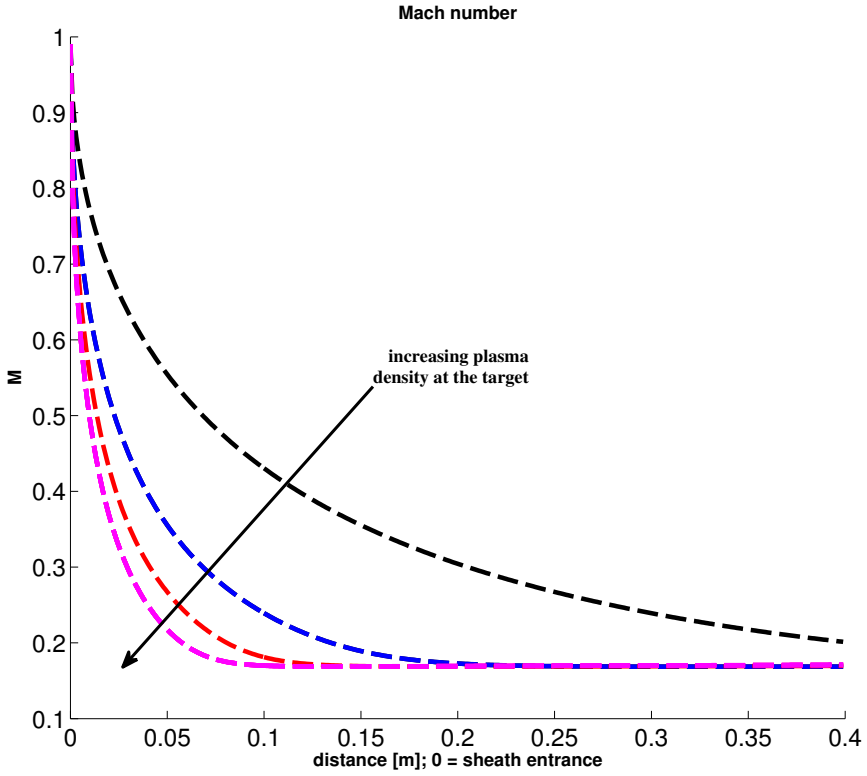

FIGURE 6.10: Mach number spread under a target density scan . Starting conditions for the simulations: $n_0 = (1:3:5:7) \times 10^{19}\ m^{-3}, T_0 = 2\ eV, R_E = 0.8$

previously as well when energy input into the plasma was varied (Figure 6.6 and Figure 6.3). Basically, the more energy reflection (whether through increase of energy reflection coefficient or biasing) the higher the Mach number and the lower the density at 2 cm in front of the target.

6.5 Characterization of the plasma acceleration zone length scale

We characterize the plasma acceleration length scale, which we regard as the effective pre-sheath length scale, by taking the e-folding length of the Mach number profiles. Results obtained under a target bias scan are shown in Figure 6.11. Results obtained under an energy reflection coefficient scan are shown in Figure 6.12.

Under a target bias scan a linear increase in the e-folding length is observed, as it is shown in Figure 6.11. This supports the previously sketched picture of change in plasma flow velocity measurements with increasing pre-sheath length, as it was shown in Chapter 3 Figure 4.7.

The rather interesting behavior of this parameter, i.e. the e-folding length, appears under an energy reflection scan Figure 6.12. Here, a saturation feature in the e-folding length appears once the target becomes a perfect energy reflector. The lack of points in the lower range if of R_E parameter is due to breaking of the exponential behavior there, when neutrals get close to their thermal regime and this is perhaps a limitation of this approach.

A limit case of a very low R_E corresponding to thermal neutrals is addressed in the following section.

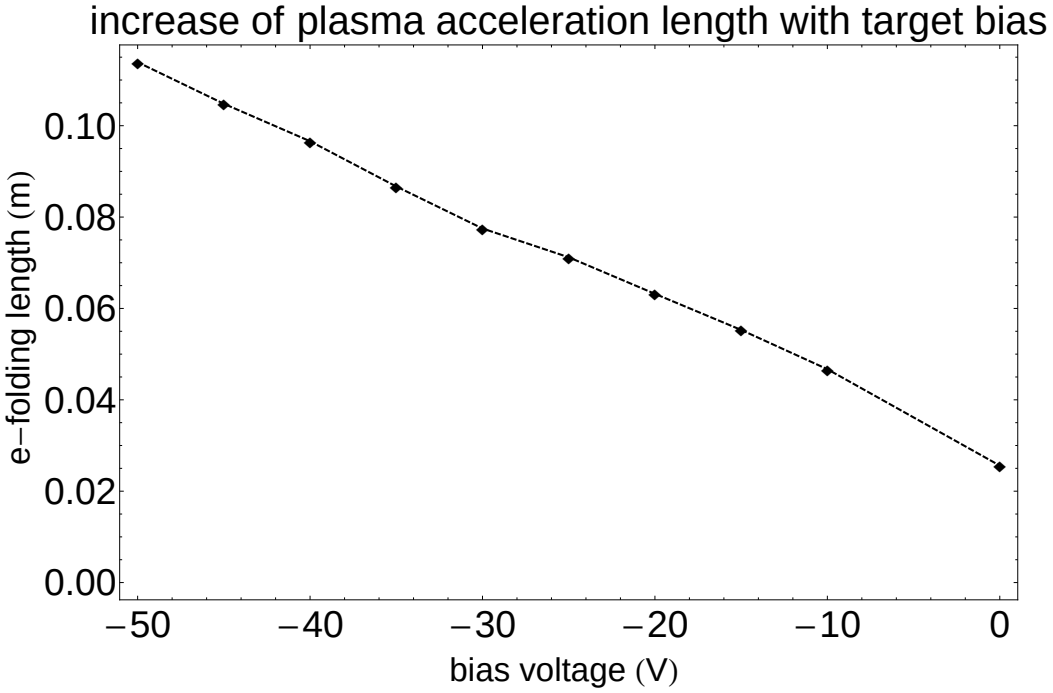

FIGURE 6.11: In this picture a characteristic of the plasma acceleration zone, the e-folding length of the velocity profiles is analyzed with respect to target bias. By subtracting the constant upstream velocity from the entire profile, an exponential decaying to zero is obtained from which the e-folding length is computed through a fitting procedure. The more energy the neutrals have the more they penetrate into the plasma and that is what this graph shows: the more negative the bias applied the larger the e-folding length. The dot in the circle was obtained at floating conditions. Technically the target is at a negative potential of $\approx 3T_e/e$ even without bias and a shift to the left should be taken into consideration.

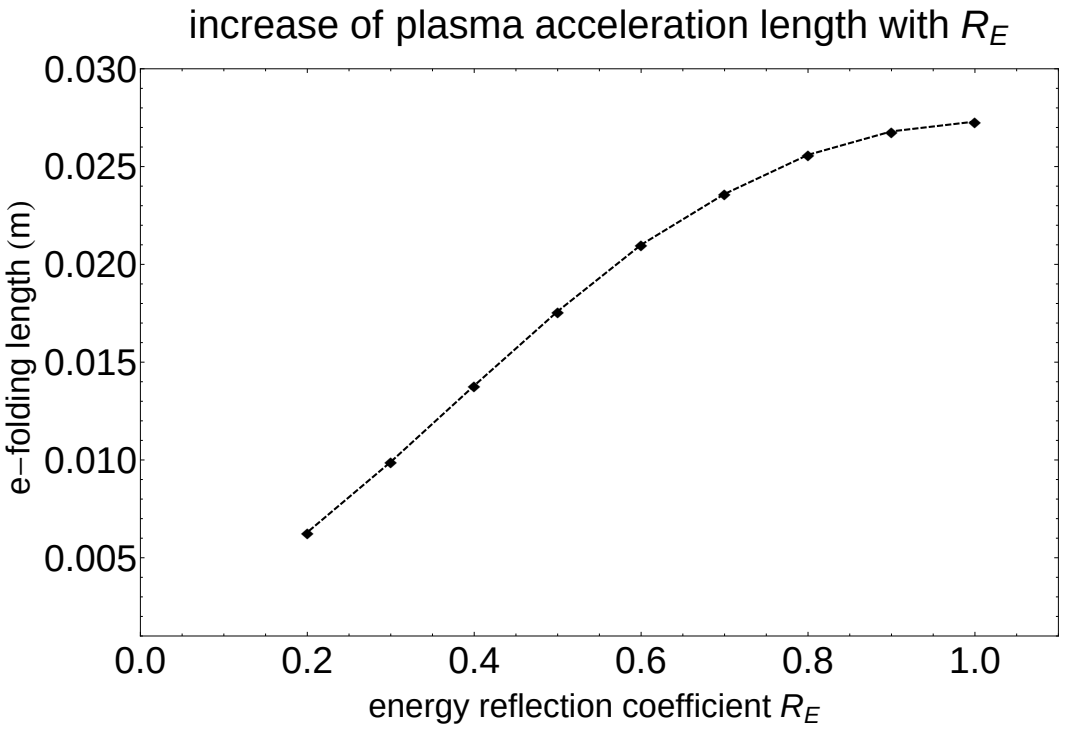

FIGURE 6.12: In this picture a characteristic of the plasma acceleration zone, the e-folding length of the velocity profiles is analyzed with respect to energy reflection coefficient. Similar to the biasing case, the more energy the neutrals have the deeper they penetrate into plasma. For low R_E, the exponential behavior breaks. This limit case corresponds to a "cushion" of neutrals that build up in front of the target and it is analyzed independently.

6.6 A limit case for thermal neutrals where conduction is responsible for peaking densities in front of the target

In this section the case of thermal neutrals is considered. Actually, the desired limit case was the one in which the reflection coefficient R_E goes to zero. However, that would create an infinite build up of neutrals in front of the target as they would have zero kinetic energy. So we follow a more realistic approach that consists of room temperature neutrals that have been thermalized at the target surface before returning into the plasma. This allows the creation of a so-called "cushion" in front of the target, of a very high density (higher than plasma density), where energy and momentum are being removed from the plasma, as shown in Figure 6.13.

An important distinction from the other simulations is being made by the absence of the neutrals in the most part of the upstream plasma. As a result, there is hardly any acceleration happening there. Conduction becomes important and that is what actually peaks the density profile near the target. The momentum flux is nearly constant up to the meeting with the "cushion" zone and while temperature decreases due to conduction the density needs to increase in order to keep the momentum flux constant. In order to verify this assumption a simulation run where parallel conduction coefficient is set to zero flattens the density profile, as shown in Figure 6.14. In addition, the most important terms of the RHS of the energy balance are plotted as well in Figure 6.14 where the charge exchange loss is by far the dominant loss mechanism.

This is an interesting behavior, where the mechanism revealed by the thermal neutrals in front of the target is envisaged as a possible solution for the divertor in the so called self shielding scenarios. An alternative to the thermal neutral shielding is represented by the vapor shielding in a case of a liquid wall divertor. However, this behavior has not been observed experimentally in the linear plasma generator, where most of the times a rarefication happens near the target due to plasma acceleration.

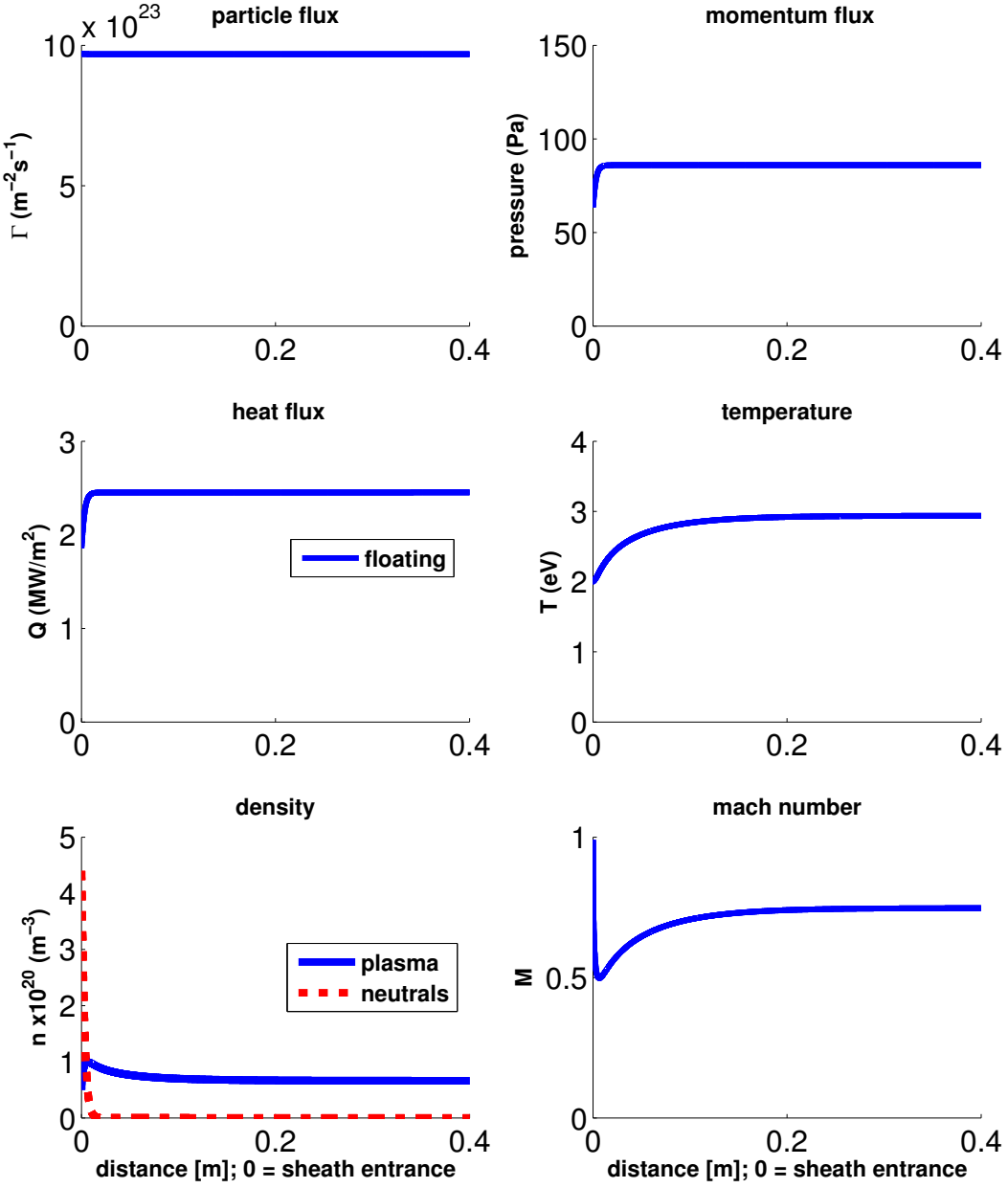

FIGURE 6.13: In this picture the case of thermal neutrals at the target is considered. The neutrals are assumed to be at 300 K, while the other starting conditions are $n_0 = 5 \times 10^{19}\ m^{-3}, T_0 = 2\ eV, R_N = 1$. The neutrals build up in front of the target and form a "cushion" that stops the incoming plasma. Their absence in the balance equations in the upstream area make most of the plasma profiles flat, apart from the temperature one which is dominated by conduction in the present case. As a result, a peaking density near the target is observed.

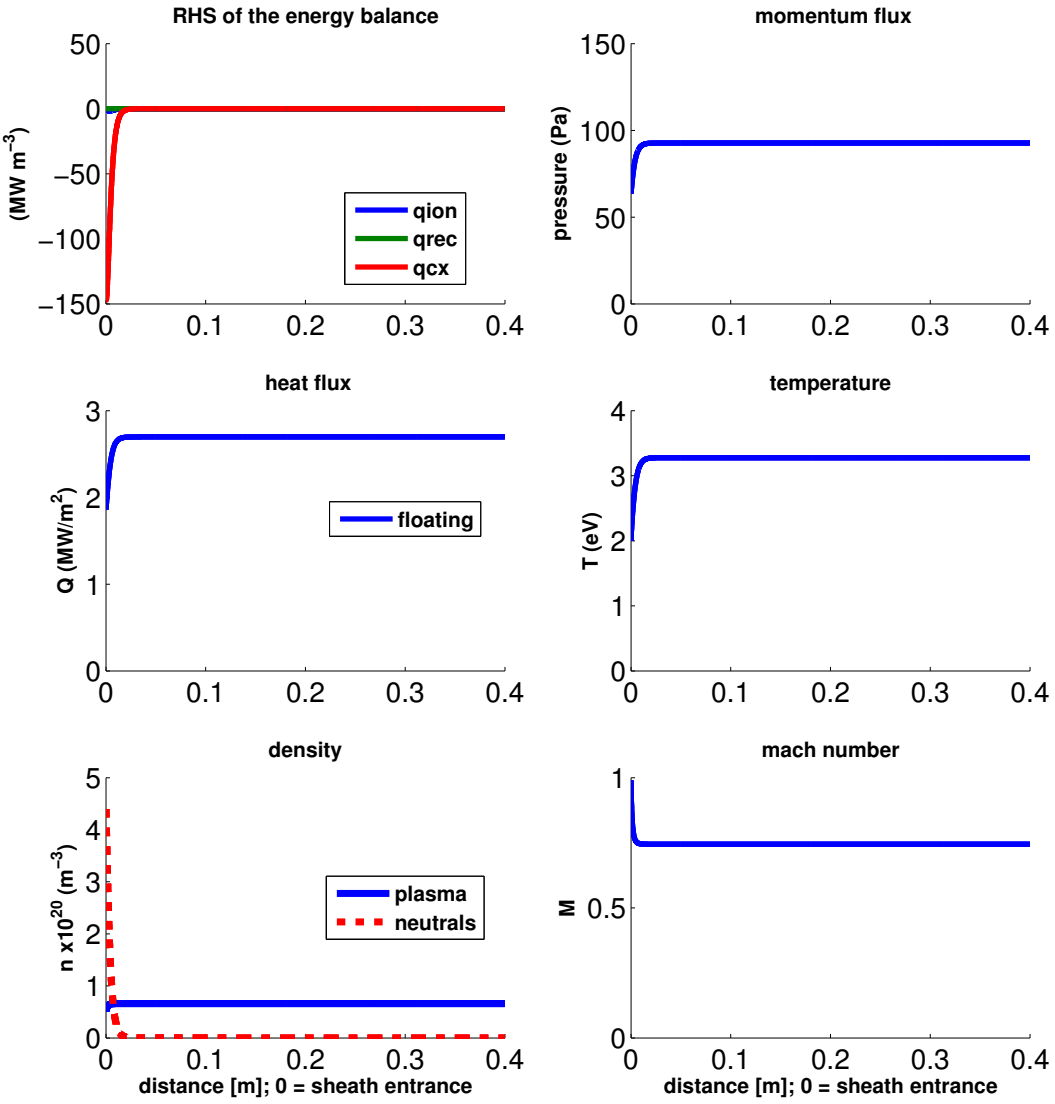

FIGURE 6.14: In this picture the case of thermal neutrals at the target is considered similar to the case in Figure 6.13, but without conduction in the plasma, that is a very small $k_{\parallel}$. Limiting the conduction effect resulted in straight profiles in the upstream plasma, with changes present when the neutrals are present as well. In addition, from the RHS of the energy balance equation plot it can be observed that the volumetric heat loss via CX is the dominant mechanism that cool the plasma near the target.

6.7 Target heat loads analysis

The effect on power density transferred to the wall as well as the kinetic energy of the incident heavy particles is evaluated as a function of the energy reflection fraction, plasma conditions and plasma sheath voltage. Figure 6.15 shows three curves that characterize the convective energy of the plasma, electrons and ions, at the sheath entrance, the energy deposited on the target by the heavy particles and the energy deposited on the target due to ion neutralization. Figure 6.16 shows the same profiles, apart from the neutralization energy, as a function of bias this time.

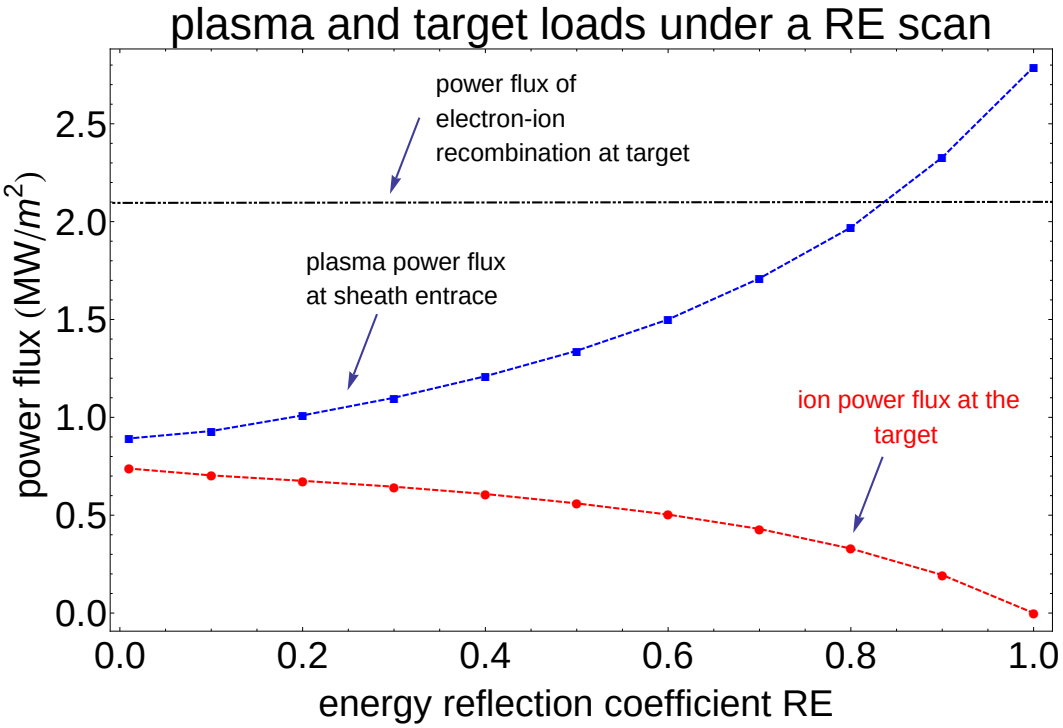

FIGURE 6.15: In this figure the plasma and target loads are assessed as a function of the energy reflection coefficient R_E in a floating case. The plasma upstream conditions, temperature and energy flux have been fixed at 1.5 eV and 1.2 MW/m^2 respectively. For a perfect reflecting target there is virtually no power delivered to it apart from the electron-ion recombination part which at this low plasma temperature values represents a considerable amount. Here $T_i = T_e$ and therefore the above graph should be viewed as an inferior limit of the potential loads.

It is seen that the energy supplied by the plasma to the plasma sheath increases strongly with reflectivity as more energy is feeded back via the neutrals while at the same time the energy deposited to the target via the ion channel becomes virtually zero for a perfect reflectivity case. Under perfect reflectivity, energy can only escape via the neutrals that have acquired the kinetic energy of the local ions and the result is that the energy confinement time goes up near the target. It seems that we have ended up in a regime of strong "power recycling".

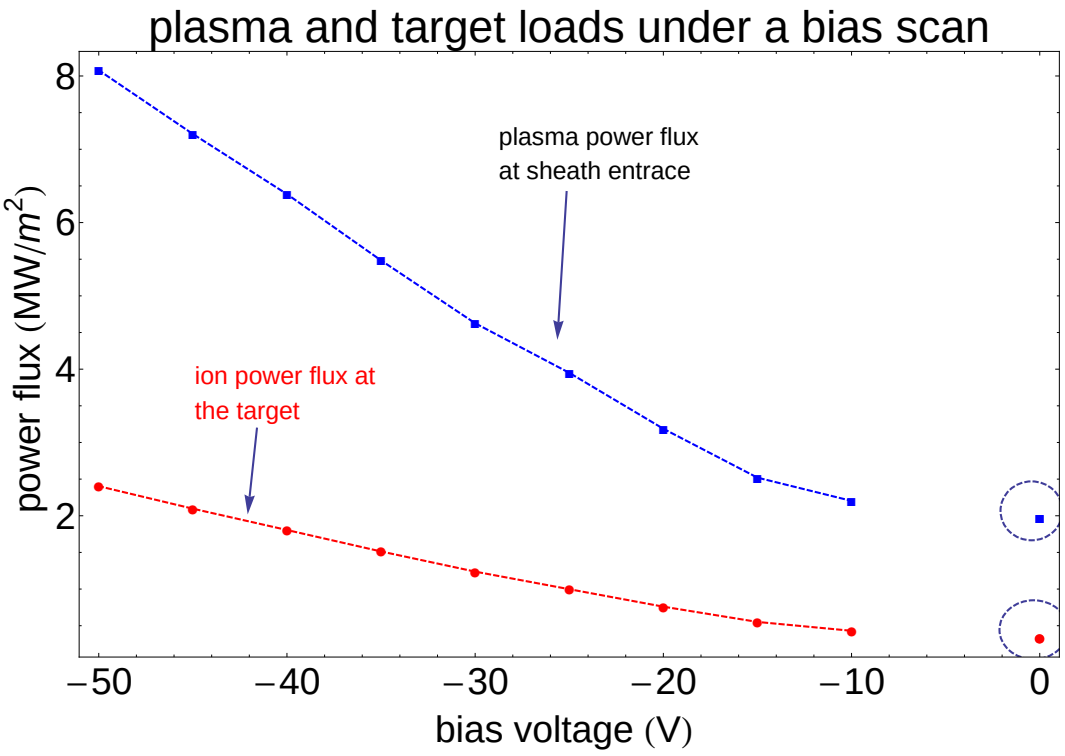

FIGURE 6.16: In this figure the plasma and target loads are assessed as a function of the other energy enhancing factor: the biasing voltage. The energy reflection coefficient $R_E = 0.8$ and plasma upstream conditions, temperature and energy flux are again fixed at 1.5 eV and 1.2 MW/m^2, respectively. Again $T_i = T_e$ and therefore the above graph should be viewed as an inferior limit of the potential loads. Technically the target is at a negative potential of $\approx 3T_e/e$ even without bias and a shift to the left should be taken into consideration.

The energy of the heavy particles, the ions, can be directly inferred from the red curve: what is not deposited goes back into the plasma. It is noted that at these low plasma temperatures (< 5 eV), the amount of energy delivered due to ion neutralization should not be neglected. In fact, it is dominant as opposed to present day tokamaks where it is often a refinement, a detail, as at e.g. 20 eV divertor plasma temperature each pair brings 140 eV kinetic energy.

Interesting is the non-linear drop of the ion power flux to the target. This is due to the response of the plasma to the energy reflection. For example, not taking the plasma response into account, one would have expected a drop in ion power flux of 80% at $R_E = 0.8$, whereas the simulations predict a smaller drop of $\sim 50\%$.

For the other case analyzed in this section, i.e. a bias scan, we see an increase with biasing for both plasma power flux at the sheath entrance as well as the power delivered to the target. In this scan, the effect of R_E is dominant as the energy of the ions is roughly $2T_i + eV_{sheath}$, thus predominantly determined by the sheath energy. The

response of the plasma affects the ion temperature, which will only be important at the lower bias voltages.

6.8 The effect of particle and energy reflection in argon

Having established that plasma heating due to energy reflection at the target is significant in the hydrogen - tungsten system, we ask ourselves how important it is for argon on tungsten. Although the underlying kinetics should be significantly different (e.g. the velocity of the argon neutrals is a factor 6 smaller at the same energy reflection, so the penetration depth should be accordingly smaller), experiments in Pilot-PSI indicated that the effect should be similar for hydrogen and argon. This makes the argon system an interesting benchmark for the present 1D modeling.

Figure 6.17 shows typical plasma profiles for argon while having hydrogen as a reference for the same initial conditions. We see that the argon acceleration (or pre-sheath) length scale is significantly smaller compared to hydrogen. Fitting the velocity profiles with exponential decay functions yielded a factor of 2 difference. We stress that this is less than the difference in velocity of the reflected neutrals factor of ~ 6.

After applying the same reasoning with the energy exchange in between neutrals and ions matching the equilibration term due to ion electron Coulomb collisions, the results obtained from an Ar simulation predict a poor coupling between ion and electron temperature. In order to better compare the increase along the axial distance from the target the presumed ΔT is normalized to the total amount of energy received by the ions from the neutrals ΔE , as shown in Figure 6.18. In this way you would expect to have similar profiles for the two cases. Nevertheless, very large differences are still observed. From the simulation point of view the Argon behavior is fully consistent with the formula dictating it 5.13.

However, we again took an energy reflection coefficient $R_E = 0.8$ whereas the energy reflection for argon will be significantly smaller than for hydrogen due to its higher mass. We didn't find precise values for R_E in the low energy range, that is $< 10\ eV$, but guessed that it could be $R_E \approx 0.4$ on basis of the mass ratio between argon and tungsten. If we use this value in a biasing case of $V_{\text{bias}} \approx -20\ V$, this would indicate a smaller temperature imbalance of ~ 10 eV. We note that the master thesis of N. den Harder [6] reports temperature imbalances of up to 8 eV on basis of spectroscopy on argon ion lines.

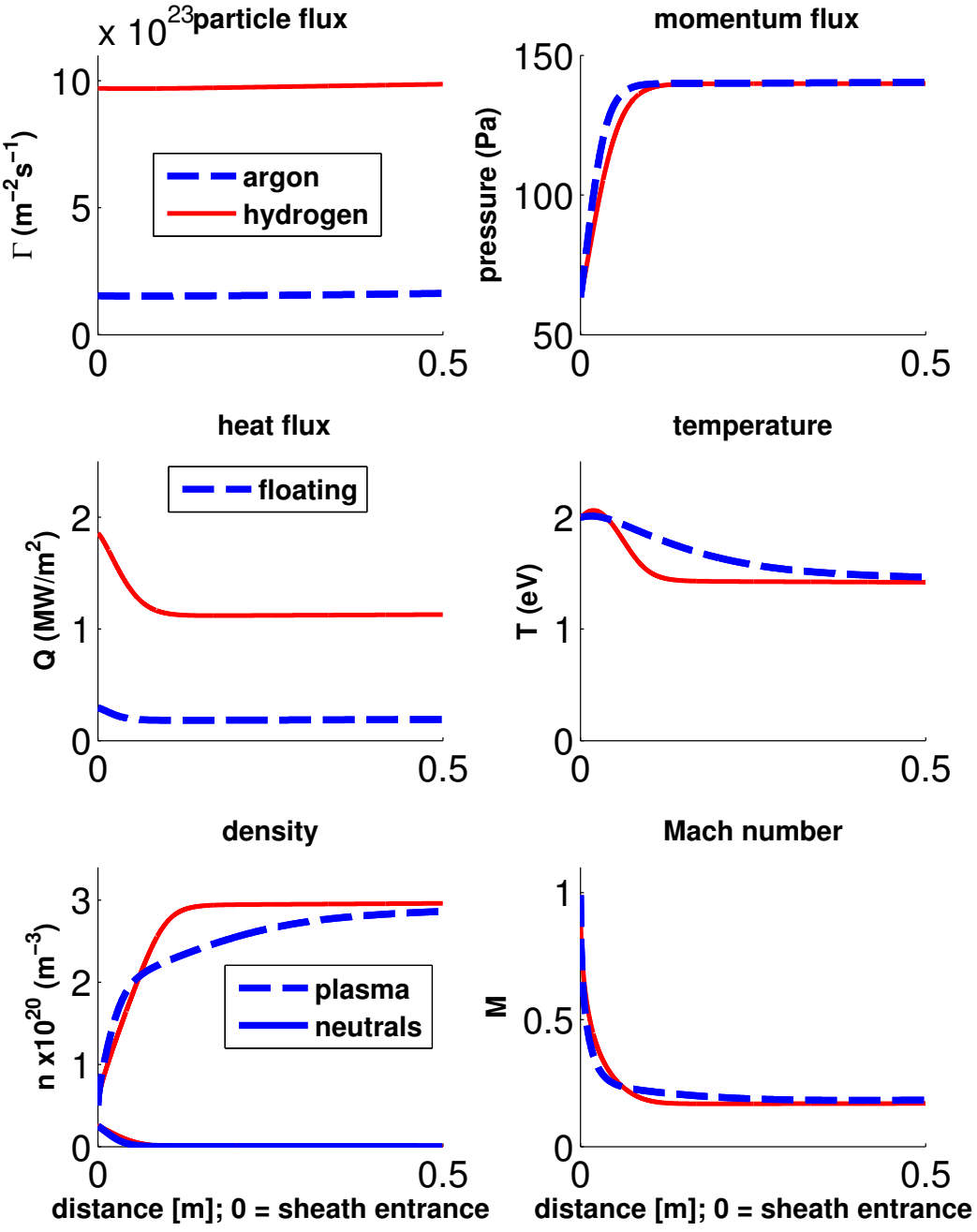

FIGURE 6.17: A simulated argon plasma -blue- with hydrogen plasma profiles as reference in red for the same starting conditions: $n_0 = 5 \times 10^{19}\ m^{-3}, T_0 = 2.0]\ eV, R_E = 0.8, R_N = 1$.

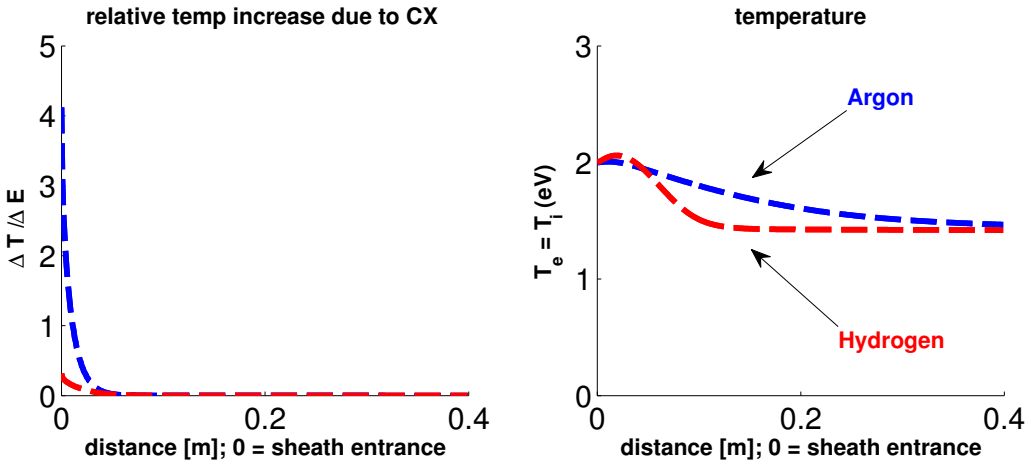

FIGURE 6.18: In this figure a comparison between an Argon and Hydrogen plasma behavior is shown with respect to plasma temperature profiles. The initial conditions at the target are $n_0 = 5 \times 10^{19}\ m^{-3}, T_0 = 2\ eV, R_E = 0.8, R_N = 1$ for both Ar and H in a floating case. The relative increase in temperature corresponds to $\approx 12\ eV$ increase in absolute value for the Ar ion temperature with respect to the electron plasma temperature and to $\approx 1\ eV$ in the H case.

Chapter 7

Transition towards a 2-fluid model

A 2-fluid has been investigated as well. The results are shown in Figure 7.1. One can see immediately that the solutions are unstable. Hypersensitivity to the initial conditions chosen for T_e and T_i is found, with both of these profiles exploding in the immediate plasma region in front of the target due to the destabilizing effect of the equilibration term. A change to a time dependent system is envisaged to stabilize the present behavior [17], however it was not possible within the time boundaries of this project. For completeness, the set of two fluid plasma equations that were formulated follows in the remaining of this chapter.

We follow the approach in the paper of Kawamura et al. [18] for the 1D fluid equations describing the divertor plasma. This is an extension of the model presented in Chapter 5.

Density and momentum equations 7.1.

$$\begin{aligned} \frac{d}{dx}nv &= K_{\text{ion}}nn_n - K_{\text{rec}}n^2 \\ \frac{d}{dx}(m_i nv^2 + n(T_e + T_i)) &= m(v_n - v)K_{\text{cx}}nn_n - mvK_{\text{rec}}n^2 \end{aligned} \tag{7.1}$$

Currently, there is only one momentum equation that accounts for both ions and electrons together, but with different temperatures in the static pressure term. Future separation of the momentum equation in two parts is envisaged as well. However, an initial reduced complexity of the overall system of equations is preferred.

Energy conservations for electrons and ions 7.2.

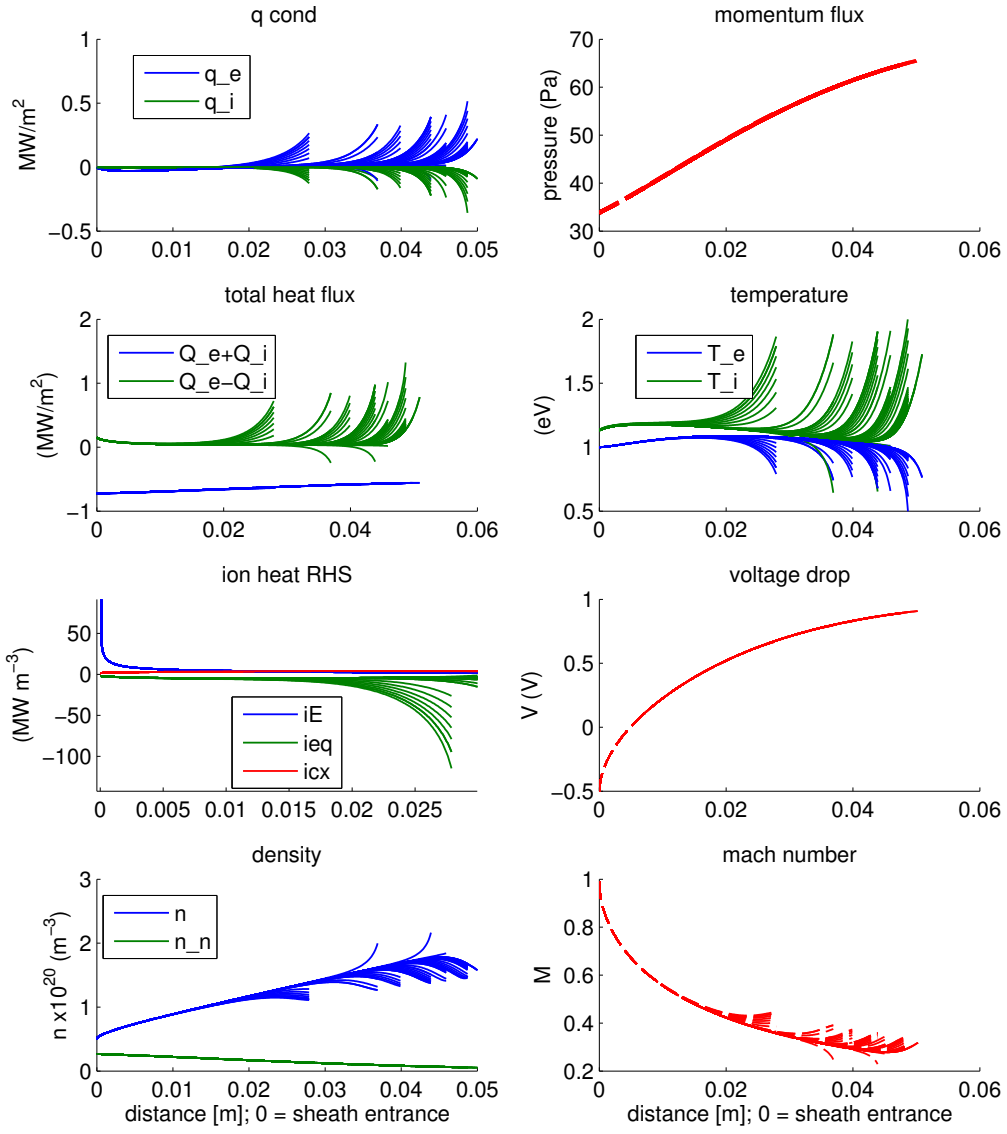

FIGURE 7.1: Plasma profiles for very small variations in the starting values of T_e and T_i

$$\begin{aligned}
\frac{d}{dx}(\frac{5}{2}nvT_e - k_{||e}\frac{dT_e}{dx}) &= +env\frac{d\Phi}{dx} - \frac{3m_e n}{m_i}\nu_{\text{eq}}(T_e - T_i) - E_{\text{ion}}K_{\text{ion}}n_n n - K_{\text{rec}}n^2\frac{3}{2}T_e \\
\frac{d}{dx}(\frac{m_i n v^3}{2} + \frac{5}{2}nvT_i - k_{||i}\frac{dT_i}{dx}) &= -env\frac{d\Phi}{dx} + \frac{3m_e n}{m_i}\nu_{\text{eq}}(T_e - T_i) + \\
&\quad - K_{\text{rec}}n^2(\frac{1}{2}mv^2 + \frac{3}{2}T_i) + K_{\text{cx}}n_n n(E_{\text{refl}} - (\frac{3}{2}T_i + \frac{1}{2}m_i v^2))
\end{aligned} \tag{7.2}$$

where the electric potential was denoted by Φ. The heat conduction coefficients and temperature equilibration coefficient are given by $k_{||e} \approx 3836T_e^{5/2}$, $k_{||i} \approx 156T_i^{5/2}$ and

$\nu_e q = 2.9{*}10^{-12}\, n\, ln\Lambda\, T_e^{-3/2}$ [10]. The new terms in the RHS of the energy balance equations are given by the equilibration energy density Q_{eq} and the presence of an electric field E in the pre-sheath. The equilibration term is defined as $Q_{\text{eq}} = \frac{3m_e n}{m_i}\nu_{\text{eq}}(T_e - T_i)$, that is, thermal equilibration collisions between electron and ions give an ion heating term. The electric field term $-eEnv$ is simply the energy transfer from electrons to ions as a result of the ambipolar electric field, where $E = -\frac{d\Phi}{dx}$.

Finally, the last equation is given by the Ohm's law, or electron momentum conservation assuming local ambipolarity 7.3.

$$e\frac{d\Phi}{dx} = \frac{1}{n}\frac{dnT_e}{dx} + 0.71\frac{dT_e}{dx} \tag{7.3}$$

In order to simplify the previous set of equations into a set of 1$^{\text{st}}$ order ODE, the following variables are introduced; flux $C_1 \equiv nv$, momentum flux $C_2 \equiv m_i n v^2 + n(T_e + T_i)$, electron and ion energy fluxes $C_3 = 5nvT_e/2 - k_{||e}dT_e/dx$ and $C_4 = m_i n v^3/2 + 5nvT_i/2 - k_{||i}dT_i/dx$.

Therefore, the fluid equations can be rewritten with these variables in equations 7.4.

$$\begin{aligned}
\frac{dC_1}{dx} &= K_{\text{ion}} n_n n - K_{\text{rec}} n^2 \\
\frac{dC_2}{dx} &= m(v_n - v) K_{\text{cx}} n n_n - m v K_{\text{rec}} n^2 \\
\frac{dC_3}{dx} &= +env\frac{d\Phi}{dx} - \frac{3m_e n}{m_i}\nu_{\text{eq}}(T_e - T_i) - E_{\text{ion}} k_{\text{ion}} n_n n - K_{\text{rec}} n^2 \frac{3}{2} T_e \\
\frac{dC_4}{dx} &= -env\frac{d\Phi}{dx} + \frac{3m_e n}{m_i}\nu_{\text{eq}}(T_e - T_i) + \\
&\quad + K_{\text{cx}} n_n n (E_{\text{refl}} - (\frac{3}{2}T_i + \frac{1}{2}m_i v^2)) - K_{\text{rec}} n^2 (\frac{1}{2}mv^2 + \frac{3}{2}T_i) \\
\frac{dT_e}{dx} &= \frac{1}{k_{||e}}(\frac{5}{2}nvT_e - C_3) \\
\frac{dT_i}{dx} &= \frac{1}{k_{||i}}(\frac{1}{2}mnv^3 + \frac{5}{2}nvT_i - C_4) \\
e\frac{d\Phi}{dx} &= 1.71\frac{dT_e}{dx} - \frac{T_e}{C_2 - 2m_i v C_1}(2m_i v\frac{dC_1}{dx} - \frac{dC_2}{dx} + n\frac{dT_e}{dx} + n\frac{dT_i}{dx})
\end{aligned} \tag{7.4}$$

Chapter 8

Conclusions and Implications for ITER

In this thesis we have investigated what happens if plasma ions reflect as energetic neutrals from (high-Z) metallic surfaces and subsequently interact again with the upstream plasma. The emphasis was on the changes in the plasma. It was observed that under the high density and low temperature plasma conditions of the FOM linear plasma generators the plasma close to the surface is heated and rarefies as it accelerates to meet the Bohm criterion at the sheath entrance at the elevated temperature.

So let's first evaluate where the power comes from to drive the heating and acceleration. In fact, the underlying mechanism is not taken into account in the present modeling but is simply imposed by taking the Bohm criterion at the sheath entrance. What will happen in reality, is that the plasma sheath acts as a filter for high energy electrons. This will cool the electrons near the target and maintains the ion accelerating electric field over the sheath. So power is transferred from the electrons to the ions by the plasma sheath and via the neutrals reflected back into the plasma and delivered to the plasma ions. Both due to the electron cooling and the ion heating, an inequilibrium between ion and electron temperature will occur locally. It is evident that the non-Maxwellian aspect of the high energy filtering as well as the temperature inequilibrium are not captured by the present 1-fluid modeling.

Next, we ask ourselves to what extent this changes the textbook analysis of sheath physics and plasma wall interaction. In fact, what is changed is the amount of energy that can be delivered by the heavy particles to the material wall. Usually it is assumed that their entire kinetic energy is deposited. This would consist of the kinetic energy due to the acceleration over the plasma sheath, typically $3T_e$ for hydrogen, and the energy per particle in a drifting Maxwellian distribution, i.e. $2T_i$. The energy delivered per

electron is unaffected and remains $2T_e$. So per electron - ion pair it is usually assumed that $\sim 7T$ energy is delivered to the surface (assuming from now on that $T_e = T_i$). This amount is usually called the sheath heat transmission coefficient. However, if the ions can only deliver the fraction $(1 - R_E) \times 5T$ to the surface, this means that the energy per particle pair reduces to $(5(1-R_E)+2) \times T$. In a convective situation as in Pilot-PSI, where upstream $5T$ per particle pair is transported, the plasma would have to cool a little in the region close to the surface (due to the action of the sheath) to match the heat transmission of the sheath if no energy is reflected. However, as energy reflection becomes significant, heating is required for a match. We have shown that in our 1D model the changeover occurs at $R_E \sim 0.6$.

In a tokamak situation, i.e. ITER, the power delivered to the scrape off layer is a given as it is determined by the fusion power. Lets assume for simplicity that all of this power has to be delivered to the divertor surfaces (in reality a significant fraction of this power will have to be radiated away). In such a case, a decreased sheath heat transmission factor implies either higher local plasma temperatures or higher local wall fluxes. In principle, both factors lead a priori to higher wall erosion rates. A quantitative statement on the deterioration in terms of wall erosion as a function of e.g. R_E is difficult as sputtering occurs due to impurities in the plasma.

A more direct implication for ITER as well as present day tokamak devices with metallic walls (such as Asdex Upgrade and JET) is of diagnostic nature. Often particle fluxes from probe measurements are compared with infrared thermography and the sheath heat transmission factor is the key parameter to relate both. It is evident that here the energy reflection coefficient must be taken into account. However, this is currently not common and explicit practice.

For Pilot / Magnum PSI, it confirms that biasing induces acceleration near the target and plasma rarefication. In addition, due to an extended pre-sheath beyond the Thomson measuring position, it makes difficult to predict particle fluxes at the target.
Moreover, it can be the case that lower power is delivered to the target than expected, i.e. one biases at -50 V expecting 50 eV ions on the target, while most of the energy is reflected back into the plasma.

The main advices to take home are: i) inclusion of R_E in the computation of the sheath heat transmission factor γ and ii) awareness of the neutral feedback on the upstream plasma; especially when under biasing conditions the importance of both effects is increased, with the mention that in a tokamak such voltages may be given due to the parallel temperature gradients.

Appendix A

Numeric Tools

Overall the entire project 3 main ODE solvers have been used for solving the numerical systems presented. Matlab ODE solvers *ode45* and *ode15s* have been a natural approach to start with. However, advancing the complexity of the ODE system (i.e. higher number of equations or higher stiffness degree) two more numerical toolboxes were used in order to cope with, namely : the NAG toolbox for Matlab [19] and the Sundials toolbox [8] for Matlab which is based on the CVODE solvers for ordinary differential equations. It is important to note that the CVODE solver is used for solving the plasma fluid equations within the UEDGE plasma simulator [9].
Solutions obtained with BDF (backward difference scheme - Sundials) and solutions obtained via RK (Runge Kutta scheme) were the same.

Bibliography

[1] M. Bessendrot-Weberpals, H. de Blank, A. Konies, E. Poli, R. Schneider. IPP summer university 2012: Basic Plasma Physics, 2012.

[2] Francis F. Chen. An Indispensable Truth:How Fusion Power Can Save the Planet, 2011.

[3] EFDA. Limiters and Divertors. http://www.efda.org/fusion/focus-on/limiters-and-divertors/. [Online; accessed October-2012].

[4] Karl Krieger. IPP summer university 2012: Plasma wall interaction in nuclear fusion devices, 2012.

[5] A.E. Shumack. *The influence of electric fields and neutral particles on the plasma sheath at ITER divertor conditions* . PhD thesis, FOM-institute DIFFER, Nieuwegein, The Netherlands, 2011.

[6] Niek den Harder. Optical Emission Spectroscopy on the linear plasma generator Pilot-PSI. Master's thesis, Utrecht University, 2011.

[7] R Schneider and A Runov. Challenges in plasma edge fluid modelling. *Plasma Physics and Controlled Fusion*, 49(7):S87, 2007. URL http://stacks.iop.org/0741-3335/49/i=7/a=S06.

[8] Alan C. Hindmarsh, Peter N. Brown, Keith E. Grant, Steven L. Lee, Radu Serban, Dan E. Shumaker, and Carol S. Woodward. Sundials: Suite of nonlinear and differential/algebraic equation solvers. *ACM Trans. Math. Softw.*, 31(3):363–396, September 2005. ISSN 0098-3500. doi: 10.1145/1089014.1089020. URL http://doi.acm.org/10.1145/1089014.1089020.

[9] A.C. Hindmarsh T.D. Rognlien, X.Q. Xu. Application of Parallel Implicit Methods to Edge-Plasma Numerical Simulations. *Journal of Computational Physics*, 175: 249–268, 2002.

[10] P.C. Stangeby. *The Plasma Boundary of Magnetic Fusion Devices: Peter C. Stangeby*. Series in Plasma Physics Series. IoP, Inst. of Physics Publ., 2000. ISBN 9780750305594. URL http://books.google.nl/books?id=qOliQgAACAAJ.

[11] J.A. Bittencourt. *Fundamentals of Plasma Physics*. Springer, 2004. ISBN 9780387209753. URL http://books.google.nl/books?id=qCA64ys-5bUC.

[12] K-U Riemann. The bohm criterion and sheath formation. *Journal of Physics D: Applied Physics*, 24(4):493, 1991. doi: doi:10.1088/0022-3727/24/4/001.

[13] H. J. van der Meiden, R. S. Al, C. J. Barth, A. J. H. Donne, R. Engeln, W. J. Goedheer, B. de Groot, A. W. Kleyn, W. R. Koppers, N. J. Lopes Cardozo, M. J. van de Pol, P. R. Prins, D. C. Schram, A. E. Shumack, P. H. M. Smeets, W. A. J. Vijvers, J. Westerhout, G. M. Wright, and G. J. van Rooij. High sensitivity imaging thomson scattering for low temperature plasma. *Review of Scientific Instruments*, 79(1):013505, 2008. doi: 10.1063/1.2832333. URL http://link.aip.org/link/?RSI/79/013505/1.

[14] O. Marchuk and M.Z. Tokar. Modeling of supersonic plasma flow in the scrape-off layer. *Journal of Computational Physics*, 227(2):1597 – 1607, 2007. ISSN 0021-9991. doi: 10.1016/j.jcp.2007.09.022. URL http://www.sciencedirect.com/science/article/pii/S0021999107004299.

[15] P. C. Stangeby, J.D. Elder. A GUIDE TO THE DIVIMP CODE. http://starfire.utias.utoronto.ca/divimp/, 1995. [Online; accessed 2012-2013].

[16] SI Braginskii. Transport processes in a plasma. *Reviews of plasma physics*, 1:205, 1965.

[17] W.R. Fundamenski. *Tokamak edge plasma modeling using an improved onion-skin method* . PhD thesis, University of Toronto, 1999.

[18] Gakushi KAWAMURA, Yukihiro TOMITA, Masahiro KOBAYASHI, and David TSKHAKAYA. 1d fluid model of plasma profiles in the lhd divertor leg. 2009.

[19] The Numerical Algorithms Group (NAG). The NAG Library (2013). www.nag.com, 2013. [Online; accessed 2012-2013].